JGR Atmospheres

RESEARCH ARTICLE
10.1029/2024JD041606

Causes of a Lack of QBO/Solar-MJO Connection in Certain CMIP6 Models

N. E. Trencham[1,2] **and L. L. Hood**[1]

[1]Lunar and Planetary Laboratory, University of Arizona, Tucson, AZ, USA, [2]Now at: Department of Applied Mathematics and Applied Physics, Columbia University, New York, NY, USA

Key Points:

- A mechanism for modulating the Madden-Julian oscillation via QBO/solar effects on extratropical wave forcing is evaluated in 6 models
- Several necessary elements of this mechanism (e.g., the Holton-Tan effect) are found to be incompletely represented by the models
- Artificial imposition of these elements via data selection produces effects on the MJO that resemble those seen in observations

Supporting Information:

Supporting Information may be found in the online version of this article.

Correspondence to:

L. L. Hood,
lon@lpl.arizona.edu

Citation:

Trencham, N. E., & Hood, L. L. (2024). Causes of a lack of QBO/solar-MJO connection in certain CMIP6 models. *Journal of Geophysical Research: Atmospheres*, *129*, e2024JD041606. https://doi.org/10.1029/2024JD041606

Received 16 MAY 2024
Accepted 25 NOV 2024

Author Contributions:

Conceptualization: N. E. Trencham, L. L. Hood
Formal analysis: N. E. Trencham
Funding acquisition: L. L. Hood
Investigation: N. E. Trencham
Methodology: N. E. Trencham, L. L. Hood
Project administration: L. L. Hood
Software: N. E. Trencham
Supervision: L. L. Hood
Validation: N. E. Trencham
Writing – original draft: N. E. Trencham
Writing – review & editing: L. L. Hood

Abstract A connection between the quasi-biennial oscillation (QBO), solar variability, and the short-term convective climate oscillation, the Madden-Julian oscillation (MJO), in boreal winter has been found in observational data, yet it is generally lacking in current global climate models (GCMs). A proposed mechanism is changes in tropical lower stratospheric upwelling rates and static stability caused by QBO and solar UV effects on extratropical wave forcing of the stratospheric residual meridional circulation (the Brewer-Dobson circulation). The extent to which this mechanism, which operates only in boreal winter and enhances similar effects of the QBO-induced meridional circulation, is simulated in a series of GCMs participating in the Coupled Model Intercomparison Project 6 (CMIP6) is investigated. The models are found to be often lacking complete representation of several elements of the mechanism, with particular issues being QBOs that are westerly biased and weak in the lower stratosphere, insufficient solar or QBO modulation of extratropical wave activity (the Holton-Tan effect), too weak reductions in equatorial tropopause static stability in response to extratropical wave forcing, and MJOs that in some cases do not respond to these reductions. Through bypassing many of these deficiencies via data selection, it is demonstrated that effects on the MJO that resemble those found in observations (strengthening of the MJO following early winter sudden stratospheric warmings and during easterly QBO winters) can be simulated by a subset of the models. This supports operation of the proposed mechanism, and points to needed model improvements, although caveats exist and further work is needed.

Plain Language Summary The 28–29-month quasi-biennial oscillation (QBO) and solar ultraviolet variations on the 11-year and 27-day timescales have signatures that have been linked to the 30–60-day convective climate oscillation, the Madden-Julian Oscillation (MJO). However, this connection is lacking in the current generation of global climate models (GCMs). A proposed mechanism is changes in tropical lower stratospheric upwelling rates and vertical temperature gradient caused by QBO and solar UV effects on the stratospheric residual meridional circulation. The extent to which both components of this modulation is simulated via this mechanism in a selection of models participating in the Coupled Model Intercomparison Project 6 (CMIP6) is examined. Key issues with multiple models are found to be weak QBO lower stratospheric wind and temperature signals, a lack of solar/QBO modulation of wave propagation into the stratosphere, weak reductions in equatorial lower stratospheric vertical temperature stratification in response to increased wave propagation, and MJOs that are sometimes unresponsive to such reductions. Through bypassing many of these deficiencies via data selection, we show that, if all of the elements of the proposed mechanism were properly represented, a QBO/solar-MJO connection could be simulated in at least some of the models.

1. Introduction

The Madden-Julian oscillation (MJO) is the leading mode of intraseasonal tropical atmospheric variability (Zhang, 2005), and exhibits teleconnections that link changes in its phase to global variations in rainfall, the occurrence of tropical cyclones and large flooding events, and even to the phase of the Northern and Southern Annular Modes (see Zhang, 2013 for a review). Therefore, a better understanding of this atmospheric phenomenon, and how it is influenced by other atmospheric phenomena and conditions, should lead to enhanced numerical weather predictability on intraseasonal timescales.

In recent years, evidence for a connection between the MJO and the stratospheric quasi-biennial oscillation (QBO) during boreal winter has been found (Nishimoto & Yoden, 2017; for a review, see Martin, Son, et al., 2021; Yoo & Son, 2016). This connection is such that enhanced/suppressed MJO activity during boreal

winter tends to occur during the easterly/westerly phases of the QBO (QBOE/W). One proposed mechanism for explaining this interaction has involved the QBO-induced meridional circulation in the tropical and subtropical lower stratosphere. The resulting cold/warm anomalies around the equatorial tropopause associated with QBOE/W act to decrease/increase the static stability there, potentially causing an increase/decrease in MJO convection (Collimore et al., 2003). Further, some suggest that the QBOE-induced temperature anomalies may enhance those induced by the MJO, creating a positive feedback between lower stratospheric static stability decreases and tropospheric MJO activity (Hendon & Abhik, 2018).

However, an assessment of 30 models participating in the Coupled Model Intercomparison Project Phase 6 (CMIP6; Eyring et al., 2016) found no evidence for a sustained QBO-MJO connection (Kim et al., 2020). This is in spite of a greater number of models simulating a QBO (15 in CMIP6 vs. 5 in CMIP5), and improvements in the modeled MJOs' eastward propagation (Ahn et al., 2020; Richter et al., 2020).

In an effort to reproduce the QBO-MJO connection in models, recent nudging experiments have been performed, in which the model tropical stratospheric zonally averaged zonal winds and/or temperatures were nudged, that is, relaxed toward reanalysis, to reproduce reanalysis QBOE-QBOW wind anomalies (Huang et al., 2023; Martin et al., 2019, 2021a, 2023). The results of these experiments have been mixed, with some providing evidence for a QBO-MJO effect (Huang et al., 2023; Martin et al., 2019), and others not (Martin, Orbe, et al., 2021, 2023).

The lack of a clear connection thus far in nudging experiments could reflect insufficient realism of aspects of the model that were not directly nudged. For example, Martin et al. (2023) note that the transformed Eulerian mean (TEM) vertical velocity, w_{TEM}, in the tropical lower stratosphere, was not very well constrained by their nudging experiments. w_{TEM} largely determines the net temperature change due to both adiabatic heating and transport-induced ozone diabatic heating. This might inhibit simulation of realistic tropical static stability reductions or other consequences of the tropical heating change following wave forcing events. Alternatively, several secondary processes and feedbacks that may be important for accurately simulating the QBO-MJO connection could be inadequately represented. As reviewed by Son (2023), the latter include longwave cloud-radiative feedbacks within the MJO envelope in the upper troposphere (Sakaeda et al., 2020; Son et al., 2017), and a Kelvin-wave-like "cold cap" anomaly in the upper troposphere and lower stratosphere that further reduces static stability and enhances MJO eastward propagation across the Maritime Continent barrier during QBOE (Hendon & Abhik, 2018; Kodera et al., 2023; Lim & Son, 2022). For example, the cirrus cloud fraction over the warm pool region increases by 20%–30% during QBOE relative to QBOW (Son et al., 2017). However, with the possible exception of the MJO vertical velocity representation, Martin et al. (2023) found little evidence for biases in the modeled MJO vertical structure and cloud-radiative feedbacks that would explain the lack of a QBO-MJO connection in the four models that they analyzed.

Some studies further indicate that changes in stratospheric circulation caused by solar ultraviolet variations may also modulate MJO activity during boreal winter. Evidence for this has been found in association with variations in solar UV flux on both the 27-day solar rotational timescale, and the full 11-year solar cycle timescale (Hood, 2017, 2018; Hoffmann & Savigny, 2019; Hoopes et al., 2024). However, this solar-MJO connection is generally secondary to the QBO-MJO connection, with significant amplifications/reductions in MJO strength occurring when the solar conditions and QBO phases reinforce each other (i.e., solar minimum and easterly QBO, SMIN/QBOE, or solar maximum and westerly QBO, SMAX/QBOW), and insignificant changes when they oppose each other (SMAX/QBOE and SMIN/QBOW).

As summarized, for example, by Mitchell et al. (2015; see their Figure 1), solar forcing of stratospheric circulation at solar maximum begins with increased ozone production and UV heating in the summer and equatorial upper stratosphere, which enhances the equator-to-pole latitudinal temperature gradient and strengthens the upper stratospheric subtropical jet near the time of winter solstice. Multiple regression analyses of stratospheric ozone, temperature, and zonal wind data have supported this causal chain in both hemispheres (Hood et al., 2015; see their Figure 7). Over the following few months, planetary-scale waves tend to be refracted more equatorward (Kodera & Kuroda, 2002) and the consequent reduction of wave flux convergence at midlatitudes weakens the stratospheric residual meridional circulation (the Brewer-Dobson circulation, or BDC). The latter directly influences tropospheric weather patterns via a "polar route" (e.g., Ambaum & Hoskins, 2002; Baldwin & Dunkerton, 2001) and an "equatorial route": The weakened tropical upwelling rate causes increased ozone concentrations and anomalous heating in the tropical lower stratosphere, which changes eddy momentum fluxes

to produce changes in tropospheric circulation, including a weakening and expansion of the Hadley cell and a weakening and poleward shift of the tropospheric subtropical jet (Haigh et al., 2005; Simpson et al., 2009).

A mechanism for producing, or at least initiating, both the QBO and solar modulations of the MJO has been proposed, motivated by the fact that the QBO-MJO connection is primarily found in boreal winter, when planetary-scale waves originating in the troposphere are able to propagate upward into the extratropical stratosphere (Hood et al., 2023; hereafter HTG23). Like the QBO-induced meridional circulation mechanism of Collimore et al. (2003), this mechanism depends on dynamically forced changes in tropical lower stratospheric heating and static stability to produce effects on the MJO. However, in this case, the changes in tropical heating result primarily from enhanced/suppressed upward fluxes of extratropical waves in early winter during QBOE/W—as seen in connection with the Holton-Tan effect (Holton & Tan, 1980; hereafter HT effect)—or during SMIN/SMAX (e.g., Gray et al., 2004, 2010). The resulting accelerations/decelerations of the BDC produce cooling/heating anomalies that affect tropical lower stratospheric static stabilities at a time when they are approaching their annual minimum values. In addition, the resulting changes in eddy momentum fluxes produce changes in tropospheric circulation, including strengthening/weakening of the Hadley cell, potentially also affecting the MJO.

In support of the "stratospheric BDC/static stability" mechanism, a high inverse correlation (– 0.87) was found between early winter extratropical wave forcing anomalies and wintertime tropical lower stratospheric static stability during strong QBOE and QBOW years (Hood & Hoopes, 2023; their Figure 3b). Even if only QBOE years or QBOW years are considered separately, a high inverse correlation (– 0.8) is obtained. This supports an important role of extratropical wave forcing of the BDC in producing static stability minima in boreal winter, in addition to the QBO-induced meridional circulation, which would be relatively constant in a given QBO phase and present in all seasons. A modulation of the wave forcing by, for example, the HT effect, would then further reduce tropical lower stratospheric temperatures under QBOE conditions, favoring larger MJO amplitudes than would be produced by the induced meridional circulation alone.

In further support of this mechanism, evidence has been obtained from both observational analyses and analyses of model data for a lagged response of the MJO to relatively large wave forcing events associated with sudden stratospheric warmings (SSWs). As found by HTG23, SSWs occurring in early winter (i.e., during the period when tropical lower stratospheric temperatures are approaching their climatological midwinter minima) produce a strong and immediate reduction of zonal mean tropical 70 hPa temperature and 70–100 hPa static stability. This is followed in ∼20 days by a statistically significant increase in MJO amplitude relative to years when no SSWs occurred. In contrast, SSWs occurring in late winter produce almost no detectable static stability reduction and no increase in MJO amplitude. MRI-ESM2.0 model data with $4 \times CO_2$ forcings from the CMIP6 archive analyzed in HTG23 showed that static stability reductions following SSWs had an amplifying effect on the model MJO. 72 early winter SSWs occurring during 450 model winters were divided into two groups, one that produced relatively large static stability reductions and one that produced relatively weak reductions. As shown in Figure 8 of HTG23, the large reduction composite yielded a pronounced strengthening of the MJO peaking 10–15 days after the central date, whereas the weak reduction composite yielded no statistically significant increase in MJO amplitude.

In this paper, an initial investigation is conducted of the conditions under which certain CMIP6 models are able to simulate the mechanism proposed in HTG23 for producing the QBO/solar-MJO connection. While several aspects of this hypothesis can be disputed and other hypotheses have recently gained more attention (e.g., Huang et al., 2023; Martin, Son, et al., 2021), it has enough positive attributes to deserve an investigation of this type, in our opinion. Specifically, the results of CMIP6 experiments for six coupled GCMs are analyzed and compared with observational results obtained from ERA5 data. By compositing the data according to the QBO phase, the presence/absence of SSWs in early winter, and the occurrence of high/low DJF static stabilities around the equatorial tropopause, each step of the proposed mechanism is analyzed. In addition, an effort is made to evaluate whether targeted data selection (e.g., selecting only model years with strong/weak early winter wave forcing to simulate an artificial HT effect) can yield modulations of the MJO that resemble those seen in observations. If successful, this will provide evidence that the analyzed mechanism, if properly represented, is capable of producing a QBO/solar-MJO connection, in at least some of the models.

In Section 2, a description of the methodology employed in analyses of both models and observational data is provided. Results are presented in Section 3. A discussion of the results, caveats, and the need for future work is given in Section 4.

2. Methodology

2.1. Raw Data and Models

For the 'observational' data, 1979–2021 daily ERA5 data from the European Center for Medium-Range Weather Forecasting (ECMWF) are employed, regridded to a regular 1° × 1° latitude–longitude grid. The models chosen for analysis, details of the CMIP6 simulations analyzed, their time periods, and resolutions are listed in Table 1.

For each model, four ensemble members of the 'historical' simulation were initially analyzed (Sections 3.1–3.5) over the time period 1950–2014, labeled as the 'original' data sets. This was done in an attempt to maintain consistency with the observational data, whilst also utilizing the available data. For the analyses presented in Sections 3.6–3.8, the ensemble sizes and/or time periods were expanded, in some cases covering the full simulation time period, 1850–2014: these were labeled the 'expanded' data sets. This was done to increase the sample sizes and statistical significance.

The MRI, MPI, IPSL, HADGEM, and UKESM models were chosen based upon the relatively high strengths of their QBOs at 50 hPa (Richter et al., 2020), and the availability of daily data at the required vertical resolution. While the WACCM model did not have a strong QBO at 50 hPa, it had a well-simulated MJO, so we also include it in our analyses for comparison purposes.

Lastly, not all models ran a 365-day year with leap days. WACCM ran 365-day years with no leap days, and HADGEM and UKESM ran 360-day years. In the former case, the 29th of February was skipped over when it would have occurred. In the latter, for analyses, the days were projected onto a 365.24-day year by multiplying the day number by 365.24/360.

2.2. Data Selection

Once the required daily data were obtained, various composite time series were constructed, filtering for the phase of the QBO, the occurrence/nonoccurrence of SSWs in early winter, and high/low mean DJF static stabilities. This was done as follows: (a) daily data were sorted into yearly time series, starting on 1 July and ending on 30 June the following year; (b) algorithms based upon specific criteria were applied to select for certain years; and (c) daily data from those years were averaged together.

To select for years with QBOE/W boreal winters, different methods were used in order to assess the sensitivity of the results to the selection method (see also HTG23). Using the 'relaxed' method, a winter was considered to qualify as QBOE/W if the DJF mean of ERA5 mean equatorial zonal winds at the 50 hPa level, $[u50]_{eq}$, was less/greater than −/+0.2 m/s. Using the 'strict' method (as in HTG23), a given winter would qualify as QBOE/W if (a) there was a change from QBOW/*E* to QBOE/W occurring no later than August; (b) the ONDJ mean of $[u50]_{eq}$ was less/greater than −1/0.6 standard deviations; and (c) for no given ONDJ month would the mean of $[u50]_{eq}$ be more/less than −0.5/0.4 standard deviations. The strict method was designed to ensure that only those years were selected when the QBO was strongly easterly or westerly throughout the fall and early winter period, when tropical lower stratospheric temperatures are decreasing to a minimum.

When compared with $[u50]_{eq}$ 1979–2021 values provided by the Free University of Berlin, the ERA5 values were generally smaller in amplitude, particularly during easterly phases, and each data set yielded standard deviations of 12.7 m/s and 11.7 m/s, respectively. However, the selection of QBOE/W winters was barely affected, with the only difference being in the qualifying QBOW winters under the 'strict' method. Under this method, both data sets found 15 QBOW winters, agreeing on 13, and differing on two each. In any case, the impact upon the results discussed in Section 3 was negligible. Therefore, only results using the ERA5 winds for defining QBO phases will be reported here.

In addition to the 'relaxed' and 'strict' methods of QBO phase classification, another method, which is labeled as 'strong', was applied to the 'expanded' data sets of models MRI, MPI, and HADGEM. This was done for the purpose of investigating whether the HT effect could be enhanced by filtering for QBOE/W winters with stronger zonal winds. According to this method, monthly means were taken of the equatorial 50 hPa zonal winds, November through January, and threshold values were applied for each month. These were, for QBOE, −17 m/s, −8 m/s, and −14 m/s, and for QBOW, 15 m/s, 16 m/s, and 13 m/s, for the MRI, MPI, and HADGEM models, respectively. These values and the time interval (NDJ) were chosen to maximize the HT effect.

Table 1
Details of Model Simulations Analyzed, for Both Original and Expanded Data Sets

Model	Reference	CMIP6 simulation	Time period	Ensemble members	Horizontal resolution (lon × lat)	Vertical resolution	Model top
MRI-ESM-2.0 (MRI)	Yukimoto, Kawai, et al. (2019)	Historical	1950–2014	r1-4i1p1f1 (original) r1-9i1p1f1 (expanded)	320 × 160 (1.125° × 1.121°)	80 levels	0.01 hPa (~85 km)
MPI-ESM1-2-HR (MPI)	Müller et al. (2018)	Historical	1950–2014 (original) 1850–2014 (expanded)	r1-4i1p1f1 (original) r1-5i1p1f1 (expanded)	384 × 192 (0.9375° × 0.9375°)	95 levels	0.01 hPa (~85 km)
IPSL-CM6A-LR (IPSL)	Boucher et al. (2020)	Historical	1950–2014 (original) 1850–2014 (expanded)	r1-2,4-5i1p1f1 (original and expanded)	144 × 143 (2.5° × 1.2676°)	79 levels	80 km
HADGEM3-GC31-LL (HADGEM)	Williams et al. (2017)	Historical	1950–2014 (original) 1850–2014 (expanded)	r1-4i1p1f3 (original) r1-5i1p1f3 (expanded)	192 × 145 (1.875° × 1.25°)	85 levels	85 km
UKESM1-0-LL (UKESM)	Sellar et al. (2019)	Historical	1950–2014	r1-4i1p1f2	192 × 145 (1.875° × 1.25°)	85 levels	85 km
CESM2-WACCM (WACCM)	Gettelman et al. (2019)	Historical	1950–2014 (original) 1850–2014 (expanded)	r1-3i1p1f1 (original and expanded)	288 × 190 (1.25° × 0.95°)	70 levels	130 km

Note. Years were averaged together.

To select for years with high/low solar UV forcing, the same method as described in HTG23 was used. In this method, daily 10.7-cm solar fluxes during 1947–2021 were obtained from the solar radio monitoring program at Dominion Radio Astrophysical Observatory in Penticton, British Columbia (https://spaceweather.gc.ca/forecast-prevision/solar-solaire/solarflux/sx-5-en.php). Averages over DJF were then calculated, and those winters with averages above 150 flux units/below 85 flux units were selected as solar maximum/minimum years (SMAX/SMIN). Note that, across the models—even for the 'expanded' data sets—this same methodology, with the same years labeled SMAX/SMIN, was employed. Therefore, years 1850–1946 were disregarded by this filtering.

To select the 'central dates' of SSWs occurring in the Northern Hemisphere, the criteria of Charlton and Polvani (2007) were used, in which the zonal mean zonal winds at 10 hPa and 60°N, $[u10]_{60\,^{\circ}\mathrm{N}}$, were required to (a) change sign at some point from November to April, from westerly to easterly, (b) return to westerly for at least 10 consecutive days before 30 April, and (c) not occur within 20 days of another SSW. The first day of the winds' sign change is defined as the central date of the SSW. Further, the SSWs were classed as 'early'/'late' if their central date was on or before/after 15 January.

To select winters of high/low equatorial static stability around the tropopause level, the average daily static stabilities over 10°S–10°N, 70–100 hPa, are first calculated, following the equation (e.g., Houghton, 1977)

$$\Gamma_{\mathrm{d}}\text{-}\Gamma = \frac{g}{c_p} + \frac{\partial T}{\partial z}$$

where Γ_{d} and Γ are the dry adiabatic and actual lapse rates, respectively, $\frac{\partial T}{\partial z}$ is the vertical temperature gradient, g is acceleration due to gravity, and c_p is the specific heat capacity of air at constant pressure. Then, winters with DJF deviations from their long-term mean greater/less than $+/-0.5$ standard deviations are classified as high/low static stability winters.

To select for early SSW events with large associated static stability reductions around the equatorial tropopause, the aforementioned daily static stability values were calculated and averaged over two time periods, -15 to -5, and 0 to $+10$ days, from the central date. Those SSW events with static stability reductions between those two

time periods of greater magnitude than − 0.7 K/km were then selected, and the remaining SSW events were grouped together as having 'small' associated static stability reductions.

To create 'pseudo-QBOE/W' winters, the daily $[v^*T^*]$ 100 hPa values (see Section 3.3), averaged over 45°N–75°N, were averaged over 'early' boreal wintertime: Dec 1–Jan 30 for MPI, and Dec 15–Feb 15 for HADGEM. Those early winters with average values above/below the mean plus/minus 1.0/1.8 standard deviations were labeled 'pseudo-QBOE/W' for MPI and HADGEM, respectively. The later 'early' wintertime period was chosen for HADGEM, owing to its climatological mean static stabilities reaching their annual minimum values later in the season compared to other models and observations (see Figure 6e). The standard deviation limits were chosen to maximize the modeled HT effect while retaining a majority of model winters.

As reviewed in the Introduction, the stratospheric dynamical response to the solar cycle in the Northern Hemisphere is characterized by an initial strengthening of the stratopause subtropical jet near the time of winter solstice under solar maximum conditions (see, e.g., Figure 7c of Hood et al., 2015). For this reason, we investigate an artificial solar influence by selecting model winters in December when the zonal wind at subtropical latitudes near the stratopause is much greater than ("pseudo-SMAX") or much less than ("pseudo-SMIN") the mean for that month. This is done by taking the 'original' model data sets, and calculating the time-, zonally, and latitudinally averaged 1 hPa 20°N–40°N December zonal winds, corresponding to the approximate location of the upper stratospheric subtropical edge of the westerly jet. Years with values greater/less than the December mean plus/minus one standard deviation—calculated over all years—were then labeled as pseudo-SMAX/SMIN (Dec). To investigate whether it was possible to produce an MJO signal via this type of filtering, further pseudo-SMIN/SMAX composites were calculated, this time by taking the 'expanded' model data sets, and calculating the time-, zonally, and latitudinally averaged 1 hPa 20°N–40°N January zonal winds. Years with values greater/less than the January mean plus/minus 1.4 standard deviations were then labeled as pseudo-SMAX/SMIN (Jan).

When compositing together years with winters classified as (pseudo-) QBOE/W (pseudo-) SMIN/SMAX, or high/low static stability, day 1 (365) of each time series corresponds to 1 July (30 June) before (after) the given boreal winter. When compositing together SSW events, each yearly time series, running from day − 182 to +182, had the SSW central date as day 0.

In addition, control composite time series for each selection method were created by averaging together data from years which did not qualify as QBOE or QBOW during that winter, or as having any SSWs, or as having high or low wintertime static stabilities. For years with no SSW events, day 0 was shifted to the average central date of each type of SSW ('early' and 'late') for each data set.

2.3. OMI Calculation

As a quantitative measure of the MJO strength, the OLR-based MJO Index (OMI) was obtained for each day of each data set. For the observational data, the OMI values were taken from the daily values calculated by the National Oceanic and Atmospheric Administration (NOAA), available at https://psl.noaa.gov/mjo/mjoindex/omi.1x.txt. For the model data, a Python code, detailed in Hoffmann et al. (2021), was applied to the daily values of outgoing longwave radiation (OLR) from each model data set.

The OMI is calculated as follows. First, the spatial patterns of the two leading-order empirical orthogonal functions (EOFs) of 30–96 days and eastward filtered daily OLR values, between 20°S and 20°N, are calculated. This is done for each day of the year, using reference observational data, giving 2×366 EOFs (including leap days). The daily OLR values, between 20°S and 20°N, of the input data set are then filtered to accept periods between 20 and 96 days, and are projected onto the corresponding EOF pair for that calendar day, with the resulting principal components (PC's) labeled OMI_1 and OMI_2. The daily OMI amplitude is then calculated as $OMI = \sqrt{OMI_1^2 + OMI_2^2}$. For more details, see Kiladis et al. (2014).

2.4. Error Calculation

Since sample sizes under 30 will frequently be encountered (see Table 2) for the composite analyses, as in HTG23, confidence intervals are calculated using a method described by LaMorte (2021). According to this method, if μ is the mean value and N is the number of samples, the confidence intervals are calculated as

Table 2
The Total Number of Winters, QBOE/W Winters According to the 'Strict' Criteria and Their Ratios (Last Column), and Early(E)/Late(L) SSWs and Their Ratios Occurring During Each QBO Phase

		QBOE				QBOW				
Original dataset	No. Winters	No. Winters	ESSWs	LSSWs	LSSWs/ESSWs	No. Winters	ESSWs	LSSWs	LSSWs/ESSWs	QBOW/QBOE winters
ERA	42	11	6	5	0.83*	15	1	6	6.00*	1.36
MRI	256	44	6	22	3.67*	108	8	64	8.00*	2.45
MPI	256	10	6	5	0.83*	150	59	95	1.61*	15.00
IPSL	256	15	7	10	1.43	115	49	58	1.18	7.67
HADGEM	256	37	13	21	1.62*	127	31	54	1.74*	3.43
UKESM	256	21	9	10	1.11*	157	31	67	2.16*	7.48
WACCM	192	84	13	32	2.46	1	0	1	-	0.01

Note. Asterisks (*) indicate late/early SSW ratios which increase going from QBOE to QBOW.

$$\mu \pm t_{N-1}\frac{\sigma}{\sqrt{N}}$$

where σ is the standard deviation and t_{N-1} is a value (tabulated in the above reference), which is calculated from a t-distribution for degrees of freedom N–1.

3. Results

3.1. QBO-MJO Connection

Figure 1 shows the time series of OLR-based MJO Index (OMI) amplitudes, calculated as detailed in Section 2.3, for composite QBOE/W (blue/red) winters, classified according to the 'relaxed' criteria detailed in Section 2.2. See Figure S1 in Supporting Information S1 for the corresponding figure using a mixture of 'strict' and 'relaxed' criteria.

The observational (NOAA) data (Figure 1a) show a clear increase in OMI in QBOE relative to QBOW for approximately the entire extended boreal wintertime period, DJFM. When composited using the strict QBO criteria (Figure S1a in Supporting Information S1), the increase in OMI becomes particularly pronounced in February, significant at the 95% level. Barring a few isolated time periods, not longer than ∼10 days individually, however, the models (Figures 1b–1g, Figure S1b-g in Supporting Information S1) generally fail to show any significant differences in OMI between QBOE and QBOW. Perhaps the models which come closest to showing a significant increase during QBOE are IPSL and UKESM (Figures 1d and 1e), which show small (∼0.2) increases lasting about 2 months during DJ/JF. However, these increases generally fall below the 95% confidence level.

Therefore, in agreement with Kim et al. (2020), there is no evidence of a strong and sustained QBO-MJO connection during boreal winter for any of the models. To investigate why, individual links in the proposed QBO-MJO causal chain are examined in the following subsections 3.2–3.5.

3.2. QBO Representation

Figure 2 displays the frequency distribution of equatorial zonal–mean zonal winds at 50 hPa, $[u50]_{eq}$, for each 'original' data set. Most of the models give reasonable distributions (Figures 2b–2f), with modal positive speed ranges from +10 to +15 m/s and modal negative speed ranges between − 15 to − 20 m/s (MRI) and 0 to − 5 m/s (MPI/IPSL), with clear biases toward QBOW, and standard deviations of around 10 m/s. Of these, most exhibit a greater QBOW bias than observations, with mean $[u50]_{eq}$ values close to or exceeding +5 m/s (Figures 2c–2f). Because of this, and its stronger easterlies, the MRI model (Figure 2b) appears to provide the best representation of the QBO at 50 hPa.

The WACCM model used for CMIP6 (Figure 2d), by contrast, has a weak QBO representation at 50 hPa, with a strong QBOE bias, and relatively low $[u50]_{eq}$ speeds (-5 ± 5 m/s). We note that this model was excluded from

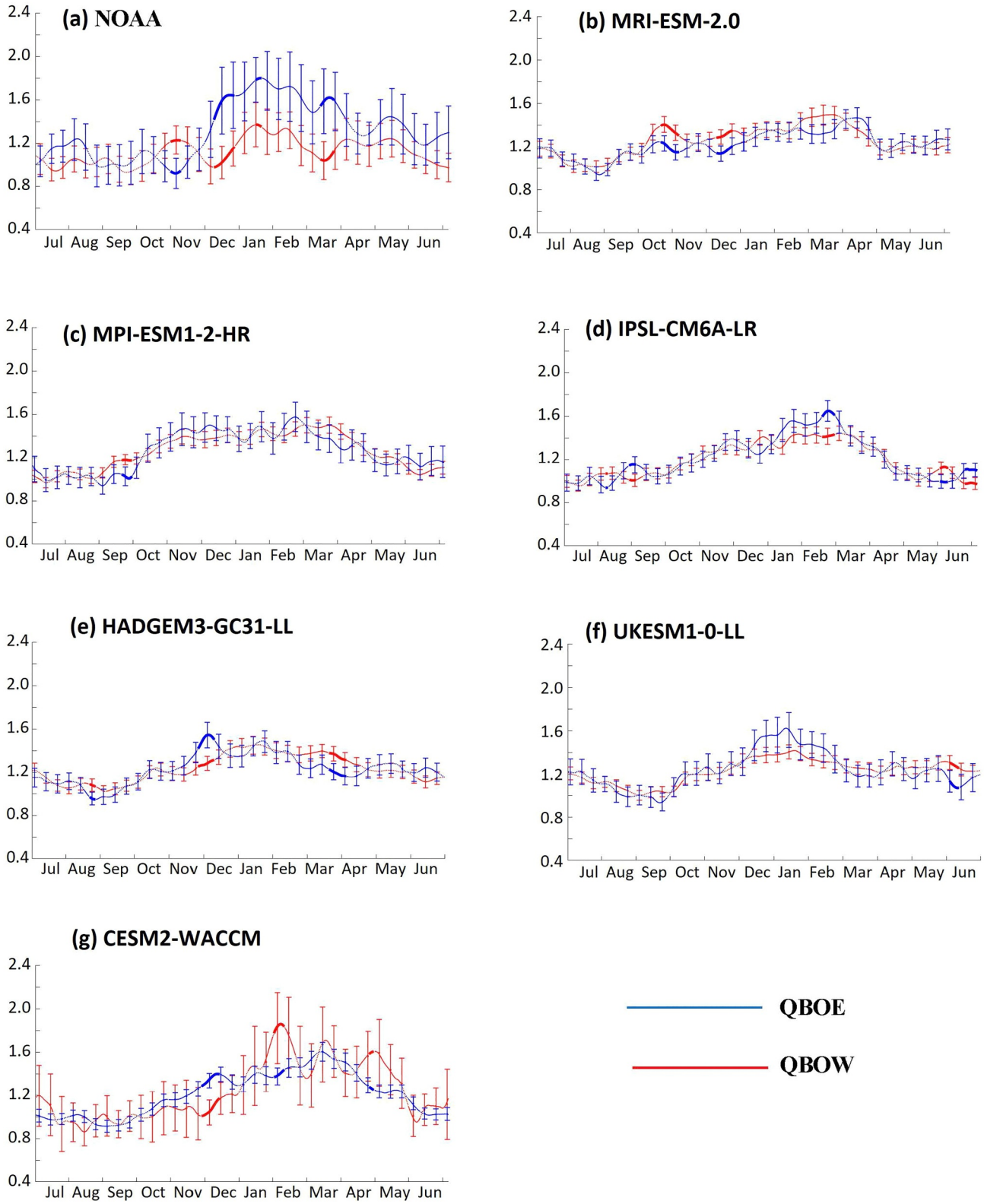

Figure 1.

further analysis by Kim et al. (2020) owing to its weak QBO representation, which did not meet their selection criteria.

Table 2 summarizes the number of QBOE/W winters, and their ratios for each 'original' data set, according to the 'strict' criteria (see Table S1 in Supporting Information S1 for the equivalent table using the 'relaxed' criteria). The QBOW bias of most models is clear from their QBOW/*E* ratios, with values ranging from 2.45 (MRI) to 15.00 (MPI), compared to 1.36 for the ERA5 data. However, these ratios generally decrease under the 'relaxed' method, suggesting that the simulated easterlies are not strong and/or persistent enough to be classed as such by the 'strict' method. The QBOE bias of WACCM is also clear, with a QBOW/*E* ratio of 0.01, which increases to 0.08 under the 'relaxed' method.

Most of the models, therefore, have QBOs which—at the 50 hPa level at least—exhibit a westerly bias, with relatively few QBOE winters, as have been found in previous studies (e.g., Richter et al., 2020). The WACCM model exhibits the opposite bias, and a very weak QBO at this level. These issues may limit the models' abilities to have an effect on the MJO, especially when considering the direct effect upon lower stratospheric static stabilities, and that the HT effect for the NH maximizes when the QBO is defined at around 50 hPa (Anstey & Shepherd, 2014; Gray et al., 2018). Previous work has found that not only the frequency distribution of zonal winds but also the spatial structure, such as the vertical extent of westerly winds and the QBO width, is important for producing a realistic HT effect (Andrews et al., 2019; Hansen et al., 2013).

That said, the model QBOs are—with the exception of WACCM—not greatly different in frequency distribution of zonal winds from that seen in observations, so a test of their ability to simulate an HT effect and, by extension, a QBO-MJO connection, is worthwhile. This is especially the case for the MRI and HADGEM models, which have a statistically reasonable number of QBOE winters (>30), even under the 'strict' criteria.

3.3. Effect of the QBO on Extratropical Wave Propagation

As already noted in the Introduction, the Holton-Tan effect, first proposed by Holton and Tan (1980), is a relationship between stratospheric equatorial and polar zonal winds that is most prominent in boreal late fall and early winter. Generally speaking, QBOE/W is associated with a weakened/strengthened NH polar vortex in early winter. The relationship has been shown to be robust, across both observational and modeling studies (see Anstey & Shepherd, 2014 for a review). Whilst the precise mechanism governing this relationship is still under investigation (Garfinkel et al., 2012; White et al., 2015; Lu et al., 2020, p. 2024), it is clear that planetary-scale wave propagation plays a dominant role, with QBOE being associated with greater propagation and convergence into the high-latitude stratosphere in early winter. This decelerates the polar vortex, and can lead to an increased incidence of early winter SSWs. In QBOW, the relationship reverses, with a strengthened NH polar vortex in early winter, inhibiting early winter SSWs, and delaying them to late winter.

SSWs are associated–through increased wave convergence driving an accelerated Brewer-Dobson circulation–with enhanced equatorial upwelling and cooling around the tropical tropopause. Hence, the HT effect has the potential to further enhance QBOE-induced reductions in static stability around the equatorial tropopause, at a time when such static stabilities are approaching their annual minimum values. It may therefore play a central role in facilitating the QBO-MJO connection (HTG23), although several secondary processes acting in the tropical tropopause layer itself, such as longwave cloud-radiative feedback (Sakaeda et al., 2020) are likely important for producing the full amplitude of the connection.

Similarly, a mechanism linking solar forcing to wave convergence, the residual circulation and zonal winds in the stratosphere has been postulated to explain the stratospheric temperature anomalies seen in response to the 11-year solar cycle (see e.g. Gray et al., 2010; Kodera & Kuroda, 2002). During SMAX, a strengthened subtropical westerly jet in the upper stratosphere causes a divergence of planetary wave flux, causing an acceleration/deceleration of the polar vortex/Brewer-Dobson circulation during boreal wintertime. Anomalous downwelling

Figure 1. Time series of composited QBOE/W (blue/red curves) OMI amplitudes, classified using the 'relaxed' criteria, based upon daily data from the (a) NOAA, (b) MRI, (c) MPI, (d) IPSL, (e) HADGEM, (f) UKESM, and (g) WACCM 'original' data sets detailed in Section 3.1. OMI amplitudes were smoothed using a 15-day running mean filter. The curves give the composite mean values, and error bars indicate the confidence intervals, calculated as described in Section 3.4. Bold, solid, and dotted curves indicate where the error bars do not overlap (considered here to be significant at the 95% confidence level), where at least one error bar does not overlap the other curve, and where neither condition holds, respectively.

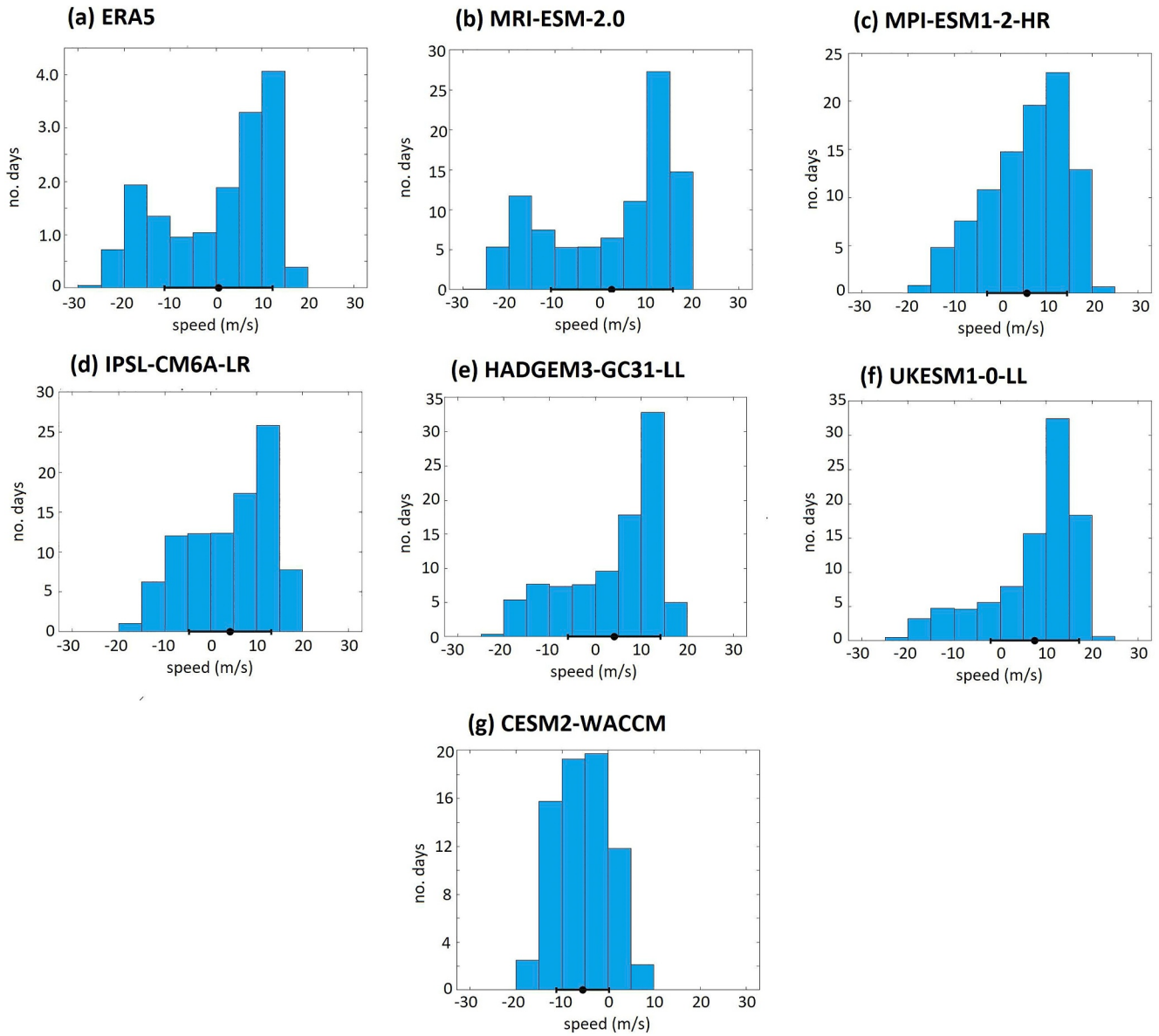

Figure 2. Histograms of $[u50]_{eq}$ values, based upon daily data from the 'original' data sets detailed in Section 2.1. The dot on the horizontal axis indicates the time-averaged value, and the horizontal error bar length in each direction indicates the standard deviation, calculated along the time dimension.

around the equatorial tropopause would then create positive temperature anomalies and increased static stabilities, inhibiting MJO convection. The converse would hold during SMIN. Both of these mechanisms warrant investigation in the models. However, as stated in the previous section, limitations in the models' representations of QBO zonal wind and temperature anomalies may make it difficult to judge how well-represented these mechanisms are.

A commonly employed proxy for the vertical component of the flux of planetary-scale waves propagating into the extratropical stratosphere is the meridional eddy heat flux, $[v^*T^*]$, at 100 hPa, averaged over 45°N to 75°N (e.g., Polvani & Waugh, 2004). As shown originally by Haynes et al. (1991) and explained further by Newman et al. (2001), this quantity is proportional to the vertical component of planetary wave flux (F_z) from the troposphere into the stratosphere. The latter is in turn a principal forcing of the effective residual meridional circulation in the stratosphere, the BDC. An increase in the eddy heat flux correlates closely with an increase in the stratospheric eddy momentum flux (proportional to F_y), which increases the Eliassen-Palm flux divergence

(e.g., Plate 4a of Newman et al., 2001). QBO-induced wave fluxes likely originate mainly in the troposphere and probably consist partly of MJO-generated Rossby waves, but may also include a stratospheric (F_y) contribution. In the present work, it is assumed that the tropospheric (F_z) component is most important and/or that F_y correlates closely with F_z.

Figure 3 shows smoothed time series of 100-hPa meridional eddy heat flux averaged over northern midlatitudes composited for QBOE/W states, using the ERA5 and model data. The eddy heat fluxes were calculated using the formula

$$[v^*T^*] = [vT] - [v][T]$$

where [] indicates the zonally averaged value (Peixoto & Oort, 1992). The corresponding figure, using a mixture of 'strict' and 'relaxed' criteria, is shown in Figure S3 in Supporting Information S1. The ERA5 data set (Figure 3a) shows a statistically significant relative increase in $[v^*T^*]$ during QBOE in late Nov/early Jan, and a subsequent significant decrease in late Jan/early Feb, and part of Mar. In contrast, none of the model data sets (Figures 3b–3g) shows a similar behavior, although statistically significant increases/decreases occur in limited time periods (e.g., for MPI and WACCM).

Table 2 provides a listing of the number of early/late SSWs occurring in each data set during each QBO phase, according to the 'strict' criteria. Table S1 in Supporting Information S1 lists the corresponding information using the 'relaxed' QBO criteria. As seen in Table 2, in the ERA5 data, 6 of 11 SSWs in QBOE occur in early winter, giving a late/early SSW ratio of 0.83. On the other hand, QBOW shows a stronger preference for late SSWs, accounting for 6 of 7 SSWs, and giving a much increased late/early SSW ratio of 6.00. While the sample size is small, this difference between QBOE and QBOW is consistent with the HT effect.

As for the models, only MPI shows a preference for early SSWs during QBOE, accounting for 6 of 11 SSWs. For all other models—as for MPI during QBOW—the most common SSWs during both QBO phases are late SSWs. That said, all of the models except IPSL and WACCM appear to show a slightly increased preference for late SSWs during QBOW, with late/early SSW ratios that increase going from QBOE to QBOW (although this preference no longer exists for MRI under the 'relaxed' criteria). WACCM also sees increased late/early SSW ratios, going from QBOE to QBOW, but the low number of QBOW winters (1) makes interpreting this result questionable.

All in all, the only model for which there is significant evidence for an HT effect is the MPI model, with small relative increases in wave forcing in early/late winter during QBOE/W, and a preference for early/late SSWs during QBOE/W. The MRI, HADGEM, and UKESM show limited evidence for an HT effect through increased late/early SSW ratios in QBOW versus QBOE, possibly related to (mostly statistically insignificant) increased eddy heat fluxes in QBOW during late winter (Figures 3b– 3e and 3f). The IPSL model shows no evidence of an HT effect, and the WACCM model cannot be evaluated due to the low number of QBOW winters (1/8) available under both criteria.

Rao et al. (2020) and Elsbury et al. (2021) both found evidence for an HT effect in most CMIP5/6 models, finding relative increases in wave convergence and corresponding zonal wind decelerations around the polar vortex during early winter (November/December–January). However, such changes were systematically underestimated by the models, and typically confined to the upper-to-mid level stratosphere. Because the mechanism of HTG23 relies upon QBOE-induced accelerations of the BDC, with enough strength and downward penetration to cause significant reductions in the equatorial lower stratospheric static stabilities, it seems unlikely that such a weak and vertically confined HT effect would be able to produce such reductions. It is unclear where the flaw in the models resides, but it may involve both stratospheric (e.g., insufficient QBO representation) and tropospheric (e.g., insufficient MJO sensitivity to static stability reductions) components.

3.4. Effect of Strong Extratropical Wave Forcing Events (SSWs) on Equatorial Temperatures

As explained in Section 3.3, increases in wave convergence around the polar vortex can—by accelerating the BDC—induce an increased upwelling and cooling around the equatorial tropopause, potentially driving more deep equatorial convection. In order to assess the representation of this phenomenon in the models in question—relevant to both the QBO- and solar-MJO connections—we focus specifically on the time evolution of static

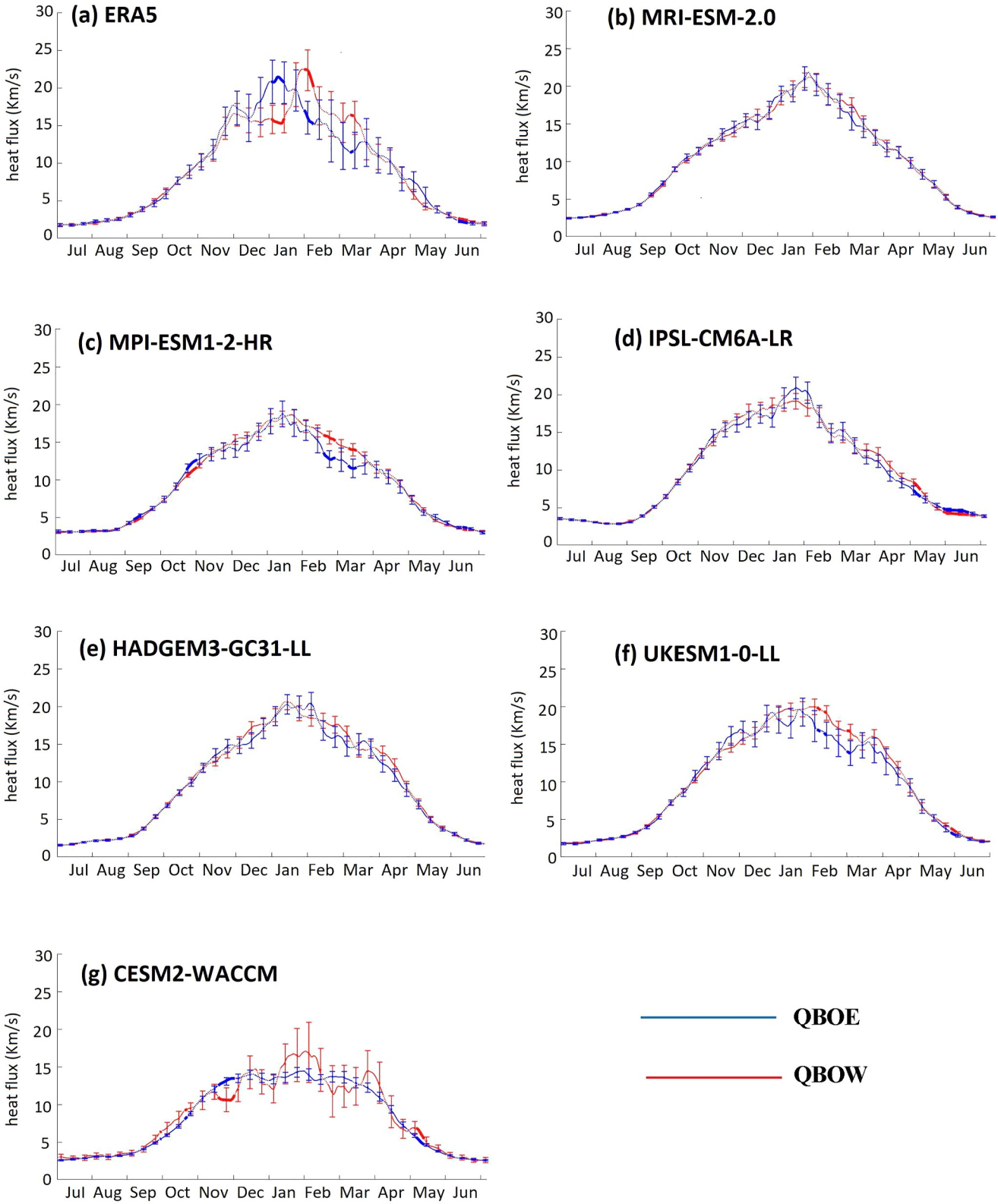

Figure 3. Time series of composited QBOE/W (blue/red curves) [v^*T^*] 100-hPa values, using the 'relaxed' method, averaged over 45°N–75°N and smoothed using a 15-day running mean filter. Data sets, solid, dotted, and bold curves, and error bars are as in Figure 1.

stabilities around the equatorial tropopause following an early SSW, as defined in Section 2.2 and displayed in Figure 4.

These are large wave forcing events, supposed to increase in frequency under QBOE/SMIN, and their timing in early winter—as equatorial lower stratospheric static stabilities approach their annual minimum—could potentially cause an amplification of the MJO (HTG23). As shown originally by Garfinkel et al. (2012), the reverse can also happen, that is, certain phases of the MJO can favor the subsequent development of an SSW by increasing the amplitudes of tropospheric planetary-scale waves. Thus, the MJO potentially acts as an agent for coupling between the polar and tropical regions of the stratosphere-troposphere system. In the current work, although no continuous circulation field from tropics to extratropics is shown, the timing of the high-latitude SSW wave forcing events and the subsequent tropical static stability reductions provides a means for inferring cause and effect.

In all data sets, with the exception of WACCM (Figure 4g), a statistically significant decrease in static stability is obtained around the equatorial tropopause, occurring around the SSW central date, and persisting for 30 (ERA5, MPI, and IPSL) to 120 days (MRI) after onset. The magnitude of these decreases is generally underestimated by the models, however, with reductions of only around −0.25 K/km (MPI, IPSL, and UKESM) or −0.5 K/km (MRI and HADGEM), compared to −1 K/km in ERA5. This may at least partly explain the lack of MJO response to such static stability reductions (see Figures S5b–g in Supporting Information S1).

The same analysis was performed for late SSWs. A similar but smaller magnitude of static stability decreases, and of shorter duration, not lasting more than 60 days (MRI), and only about 10 days in ERA5, was observed in the model and ERA5 data (Figure S6 in Supporting Information S1). This is likely due to the SSWs occurring around the annual minimum in static stability values, and thereby increasing soon after onset. Neither reanalysis nor model data showed any response in the MJO to these decreases (Figure S7 in Supporting Information S1).

3.5. Effect of Equatorial Static Stabilities on MJO Amplitude

Finally, the responsiveness of the MJO to decreases in equatorial static stability around the tropopause during boreal winter is assessed in each data set, the last essential feature in the proposed QBO/solar-MJO connection mechanism. In general, according to this mechanism, it would be expected that models with the lowest values of climatological static stability around the equatorial tropopause should show the strongest and most significant wintertime OMI increases, whereas those with the largest static stabilities should show little or no changes in MJO activity. In the ERA5 data, years with DJF static stabilities less than about 12 K/km show the largest MJO amplitudes (e.g., Figure 2b of Hood & Hoopes, 2023). However, this approximate threshold in observations may not be appropriate for some models, so high/low static stability winters are defined here as those with DJF deviations from their long-term means greater/less than ± 0.5 standard deviations (Section 2.2). It would also be expected that the strongest OMI increases should occur near or following the time of year when the model climatological static stabilities are at a minimum. In the ERA5 data, this occurs in midwinter but that may not be the case for some models.

Figure 5 displays the time evolution of OMI amplitudes, composited according to years with relatively high/low DJF static stabilities (red/blue curves). For comparison, Figure 6 shows the evolution of the composited static stabilities. While the patterns of seasonal variation in, and differences in static stabilities between, the low/high static stability composites are fairly similar across the different model data sets, there are large differences in the absolute values of static stabilities. WACCM has the lowest values (Figure 6g), with a minimum of below 10 K/km, while MRI and UKESM have the highest values (Figures 6b–6f), with no values below 11.5 K/km.

The ERA5 data show clear relative increases in OMI amplitude throughout most of DJF during the low versus high static stability winters, with confidence levels exceeding 95% during February (Figure 5a). This aligns with the period of lowest static stabilities (below 11 K/km) in January and February (Figure 6a). For the models, only IPSL, HADGEM, and WACCM (Figures 5d, 5e, and 5g) exhibit OMI increases which exceed the 95% confidence level. Of these, WACCM shows the most convincing increase, of about +0.4, and exceeding 95% for most of October, January, and February. The longest sustained period of increased OMI for WACCM occurs from January to March, which coincides with the period of lowest static stabilities (below 10 K/km) for this model (Figure 6g). MRI and UKESM show no changes in OMI (Figures 5b–5f), consistent with their relatively high minimum static stabilities (Figures 6b–6f). IPSL has moderately high minimum static stabilities (Figure 6d), but

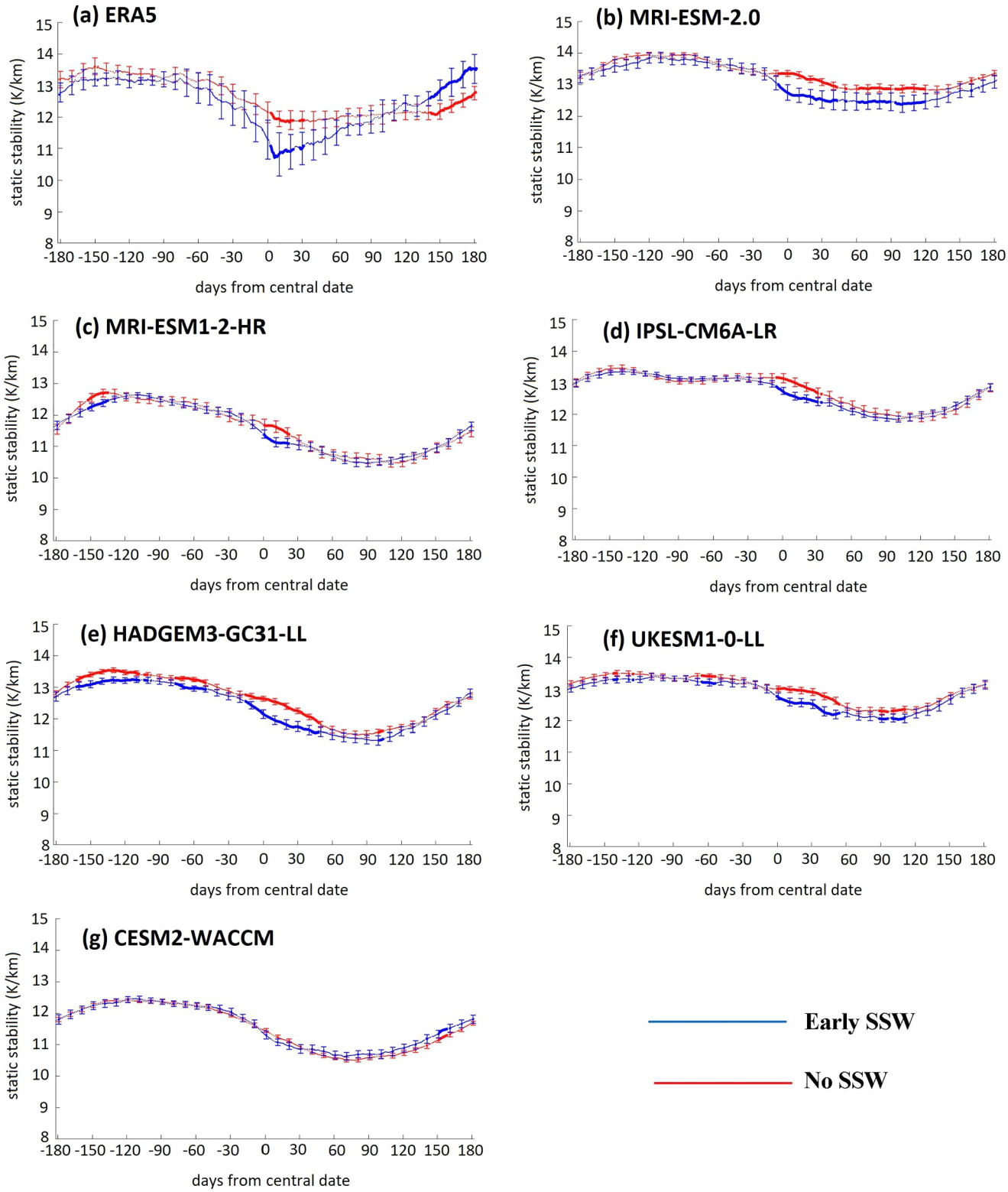

Figure 4. Time series of composited early SSW/non-SSW (blue/red curves) 70–100-hPa static stability values, averaged over 10°S–10°N, smoothed using a 15-day running mean filter. Data sets, solid, dotted, and bold curves, and error bars are as in Figure 1.

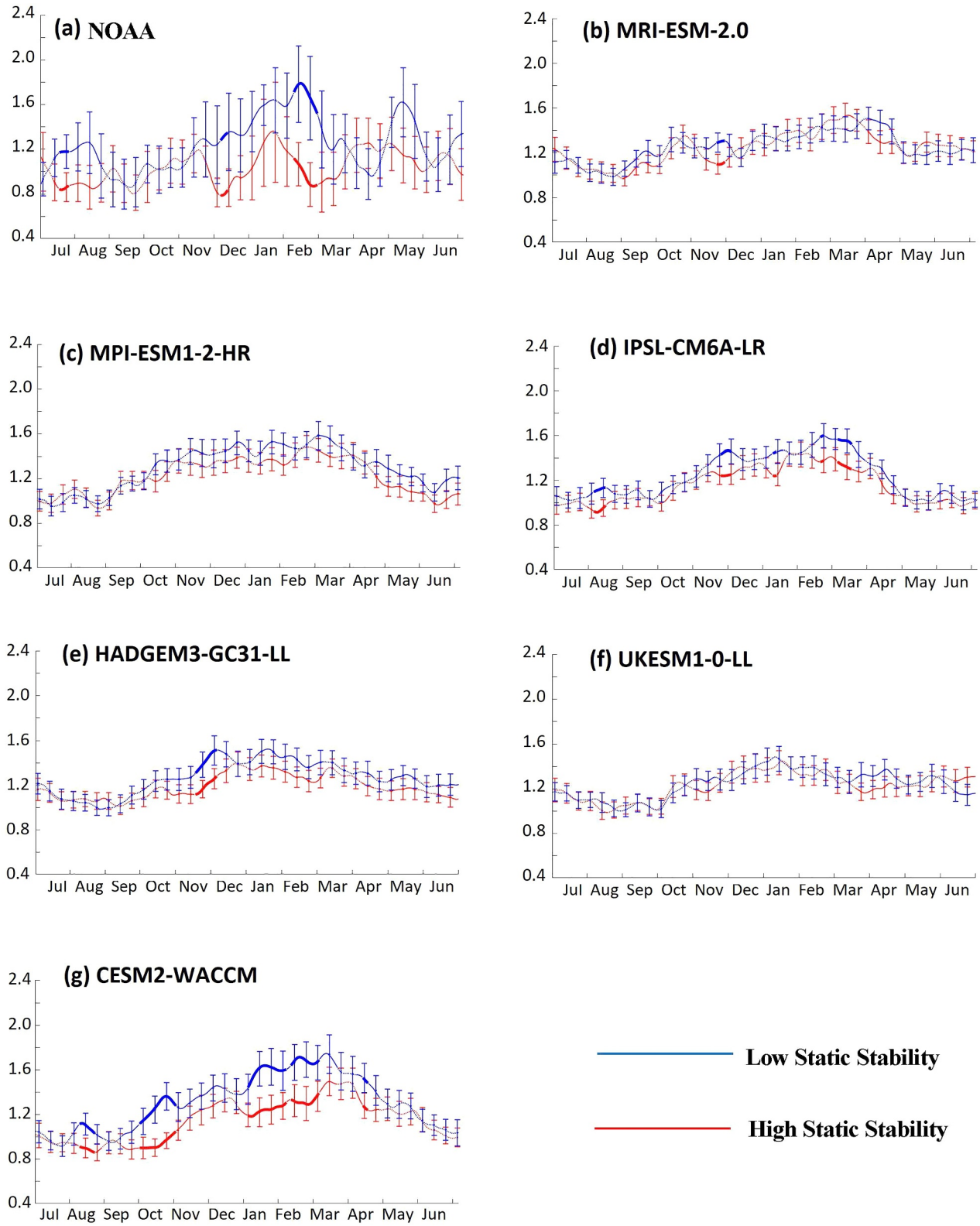

Figure 5. As in Figure 1, but for composited years with low/high DJF static stabilities.

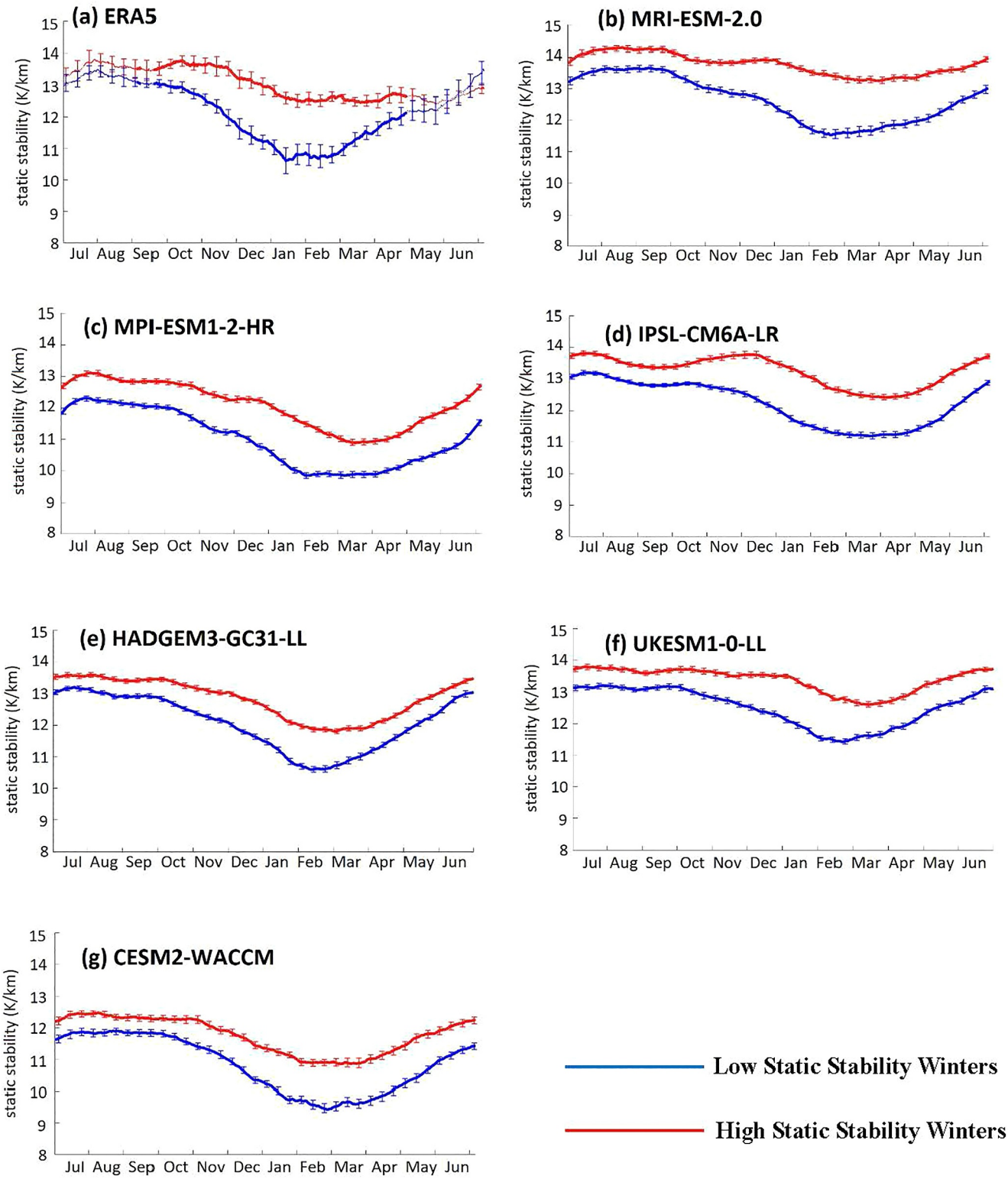

Figure 6. As in Figure 4, but for composited years with low/high DJF static stabilities.

nevertheless shows small OMI increases of about +0.2 (Figure 5d), peaking during February and March when the static stabilities are at a minimum (below 11.5 K/km). HADGEM shows small increases of about +0.2, and exceeding 95% for short periods (Figure 5e), but not obviously coinciding with its climatological static stability

minimum, which is less than 11 K/km (Figure 6e). MPI shows similar small increases (Figure 5c), but not at the 95% level, even though its static stability minimum is slightly below 10 K/km (Figure 6c).

3.6. Effect of Early SSW Events With Large Static Stability Reductions on the MJO

Thus far, the representations of each step of a potential causal mechanism behind the QBO/solar-MJO relationship (HTG23) in various CMIP6 models have been individually examined. However, it has not yet been demonstrated that this mechanism, if fully represented by the models, would reproduce the observed relationship. To this end, the effect of early SSWs with "large" associated reductions in equatorial static stability is examined in this subsection. These static stability reductions are known to be caused by accelerations of the BDC and associated increases in tropical upwelling rate. Wave fluxes that initiate SSWs originate mainly in the troposphere and consist partly of MJO-generated Rossby waves, but may also include a stratospheric (F_y) contribution.

Model SSWs are selected using the criteria outlined in Section 2.2 (i.e., reductions of more than 0.7 K/km between two time periods, from −15 to −5, and from 0 to +10 days from the central date). While it is true that the MJO can also reduce static stability in the tropical lower stratosphere at some longitudes ahead of the main convective center through its "cold cap" anomaly (Hendon & Abhik, 2018; see their Figures 1 and 2), it is not mainly responsible for the immediate reduction of zonal mean static stability that follows observed SSW central dates (e.g., Figure 4a). The condition of the MJO is not considered in the selection of model SSWs to avoid any bias of the sample.

Figure 7 displays the time evolution of 70–100 hPa equatorial static stability and OMI amplitudes, composited around the selected early SSWs, and compared to composites for years with no SSWs, for the MPI, IPSL, HADGEM, and WACCM models. These models were chosen because (a) their MJOs showed some response to reductions in static stability (previous subsection) and (b) their early winter SSWs produced significant reductions in static stability (subsection 3.3). The 'expanded' data sets described in Section 2.1 (Table 1) were used for this analysis, which increased the number of early SSWs to 335, 273, 241, and 88, respectively. Of these, 77, 35, 46, and 22 qualified as having "large" static stability reductions.

All models except WACCM (Figures 7a– 7c and 7e) show clear relative reductions in static stability of around −1 K/km, persisting for 60–90 days after SSW onset. Correspondingly, both MPI and HADGEM show rises in OMI (~0.2–0.3) around the SSW central date, significant at the 95% level, persisting for up to 30 days (Figures 7b–7f). Notably, both of these models reach relatively low static stability values of below 11.5 K/km around the central date, in contrast to IPSL, which has minimum static stabilities exceeding 12 K/km, and shows no significant rise in OMI around the central date. In the case of HADGEM (Figure 7f), the 15-day running mean MJO amplitude begins to increase more than a week prior to the central dates. This may not be a contradiction, however, since, in both observations and models, the static stability begins to decrease from about 10 days prior to the central dates.

3.7. Pseudo-QBOE/W Winters and Effect Upon MJO

It was found in the previous subsection that early winter SSWs can amplify the OMI in several models whose SSWs produce significant reductions in tropical lower stratospheric static stability, provided that a large enough static stability reduction is produced. Since early winter SSWs tend to increase/decrease in frequency during QBOE/QBOW and SMIN/SMAX, this is consistent with the proposed stratospheric BDC/tropical heating mechanism in producing the QBO/solar-MJO relationship, if properly represented in the models. To test this provisional conclusion further, the effect of imposing an artificial HT effect via data selection is investigated in this subsection. As was seen in Figure 3a, the HT effect is characterized observationally by a statistically significant relative increase in $[v^*T^*]$ at 100 hPa during QBOE in early winter, produced by a combination of both more SSWs and more minor wave forcing events. We therefore select 'pseudo-QBOE/W' winters in the model data as those with average $[v^*T^*]$ values well above (pseudo-QBOE) or below (pseudo-QBOW) the mean. While 100 hPa $[v^*T^*]$ is a measure of wave activity entering the stratosphere at northern midlatitudes, it is observed to be modulated by the QBO.

For this purpose, two models, MPI and HADGEM, are chosen due to their ability, illustrated in the previous subsection, to produce an MJO amplification following an early SSW of sufficient static stability reduction. Figure 8 shows the composited pseudo-QBOE/W time series—selected using the specific criteria given in

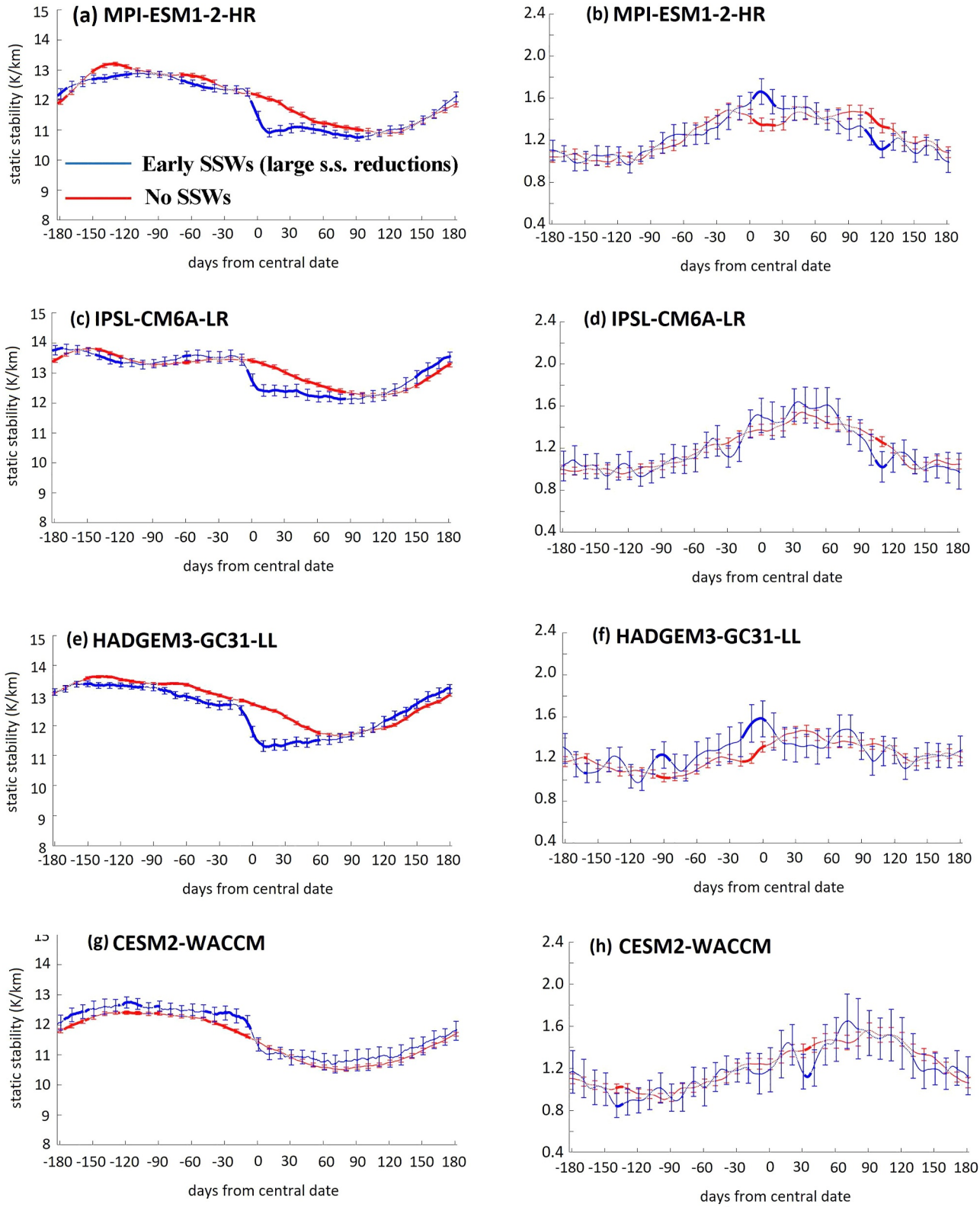

Figure 7. Time series of composited early SSWs with "large" associated static stability reductions/non-SSW (blue/red curves) (a, c, e, and g),70–100-hPa static stability values, averaged over 10°S–10°N, and (b, d, f, and h) 15-day running mean OMI amplitudes. Based upon data from the (a), (b) MPI (c), (d) IPSL (e), (f) HADGEM, and (g), (h) WACCM expanded data sets described in Section 2.1. The curves give the composite mean values, and error bars indicate the confidence intervals, calculated as described in Section 2.4. Solid, dotted, and bold curves and error bars were calculated as described for Figure 1.

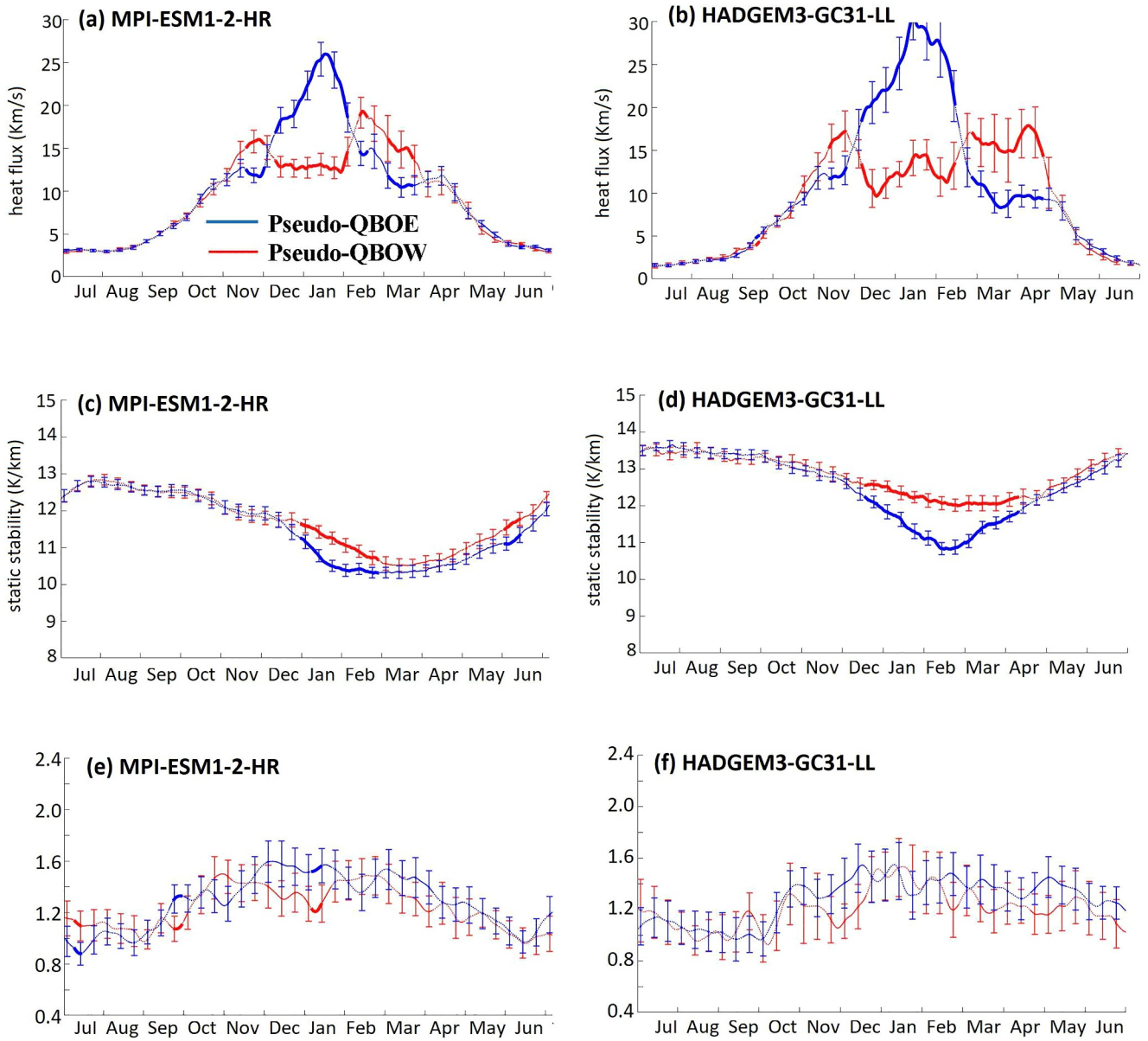

Figure 8. Time series of composited pseudo-QBOE/W winters (blue/red curves), using the 'expanded' data sets of the MPI and HADGEM models (a), (b) $[v^*T^*]$ 100 hPa 45°N–75°N values (c), (d) 70–100 hPa 10°S–10°N static stability values, and (e), (f) 15-day running mean OMI amplitudes.

Section 2.2, applied to the "expanded" data sets, defined in Section 2.1—of extratropical eddy heat fluxes and equatorial static stabilities around the tropopause, and OMI values for MPI and HADGEM. This yields 30/21 and 36/112 pseudo-QBOE/W winters, respectively, out of 820 in total in each case.

As seen in Figures 8a and 8b, large relative increases in the eddy heat fluxes over Dec 1–Jan 30/Feb 15—approximately the periods over which threshold values were applied—are obtained, significant at the 95% confidence level. Corresponding decreases are found in equatorial static stability of about -0.5 K/km, significant at 95% confidence, throughout December through February/March (Figures 8c and 8d), and small increases in OMI (~0.2) during most of Dec–Jan/Dec, and parts of Mar/Feb–May, are found, but they are seldom significant at the 95% level, likely due to the small sample sizes of most of the composites (Figures 8e and 8f). Still, given the lack of threshold values placed upon the induced static stability reductions, these relative OMI increases are encouraging, and add some evidence in support of the proposed hypothesis.

3.8. Effect of Pseudo-SMIN/SMAX and 'Strong' QBOE/W States Upon Extratropical Wave Fluxes

Lastly, we aim to test the hypothesis that properly representing the signatures of SMIN/SMAX and QBOE/W upon the zonal winds in the stratosphere will lead to a modulation of the extratropical eddy heat fluxes, similar to the observed 'Holton-Tan' effect (see Figure 3a). To this end, we turn our analysis to the 'pseudo-SMIN/SMAX' and 'strong-QBOE/W' composites, constructed as described in Section 2.2, and their effect upon the eddy heat fluxes in the lower extratropical stratosphere, illustrated in Figure 9.

For more or less all of the examined data sets, we see a clear modulation of the eddy heat fluxes by pseudo-SMIN/SMAX, with relative, significant increases during SMIN in Dec, and subsequent decreases at various Jan–Mar points (Figures 9a–9f). This contrasts with the lack of signal seen when analyzing SMAX/SMIN composites (Figure S4b–g in Supporting Information S1). The 'strong' QBOE/W composites (Figures 9g and 9h) also produce a stronger signal for the analyzed HT effects, versus when QBOE/W is constructed using both the 'relaxed' (Figures 3b–3e) and 'strict' (Figure S3b and e in Supporting Information S1) criteria. HADGEM (Figure 9h) in particular shows a marked signal enhancement, with increases in Dec, and subsequent decreases in Feb–Mar, often significant at 95%. In support of the strengthened HT effect, the late/early SSW number ratios decrease/increase under the 'strong' QBOE/W criteria for both MRI and HADGEM, compared to both the 'relaxed' and 'strict' criteria (see Tables S2-3 in Supporting Information S1).

When effects upon the equatorial static stability and MJO amplitude are analyzed (see Figures S8-9 in Supporting Information S1), we see significant corresponding decreases in static stability during pseudo-SMIN/QBOE in boreal winter across the majority of the composites (Figure S8 c–h in Supporting Information S1), leading in most cases to substantial OMI increases (~0.2–0.4, Figure S9c, d, e, and g in Supporting Information S1) at various points in winter, though not often significant at 95% confidence. It must be noted, however, that, in order to see these OMI increases, as described in Section 3.2, tighter criteria later in boreal winter needed to be placed upon the 1 hPa subtropical westerlies, requiring them to be 1.4 standard deviations above/below the climatological mean in January for the pseudo-SMAX/SMIN states. Further, noted aliasing with the QBO means further analysis —ideally removing this bias via for example, multiple linear regression analysis—is necessary.

Still, these all serve as extra evidence that if the effects of the QBO and solar cycle upon the stratospheric zonal winds were properly represented, a corresponding modulation of the eddy heat fluxes, equatorial static stabilities, and MJO can be produced in at least some of the models.

4. Discussion, Caveats, and the Need for Future Work

In Sections 3.1–3.5, each individual component of the proposed stratospheric BDC/static stability mechanism for producing the QBO/solar-MJO connection was examined, in both ERA5/observational data, and 6 CMIP6 model simulations. To summarize, the following components were found to be represented by the models to the following degrees.

- 50 hPa QBO representation: very good (MRI); good but easterlies transient (HADGEM and UKESM); fair, easterlies weak and transient (MPI and IPSL); and poor, strong easterly bias and weak (WACCM);
- QBO/solar modulation of extratropical wave fluxes: Yes but very weak (MPI and MRI); only evidence for effect of QBOW in late winter (MRI, HADGEM, and UKESM); and no real evidence/insufficient data to evaluate a QBO/solar modulation (IPSL and WACCM);
- Extratropical wave forcing of reduced equatorial static stabilities: Yes but weaker (MRI, HADGEM, and UKESM); yes but weaker and transient (MPI and IPSL); and no evidence (WACCM);
- Forcing of the MJO by wintertime equatorial static stability decreases: Strong and persistent (WACCM); weak and transient (IPSL and HADGEM); weak and insignificant (MPI); and none (MRI and UKESM).

Each model has under-represented components of the proposed mechanisms in slightly different areas. The MRI, for instance, has a very realistic 50 hPa QBO representation, a partial Holton-Tan effect, small but persistent static stability decreases in response to extratropical wave forcing, but no evidence of any modulation of the MJO by static stability decreases. Conversely, the WACCM model captures this latter component very well. But this particular model version had a weak and strongly easterly-biased QBO, and no evidence of a modulation of equatorial static stabilities by extratropical wave activity or a Holton-Tan effect, although the latter is difficult to verify due to a low number of QBOW winters. We note that the QBO representation of this model has recently been improved considerably by increasing vertical resolution (D. Marsh, private communication, 2024).

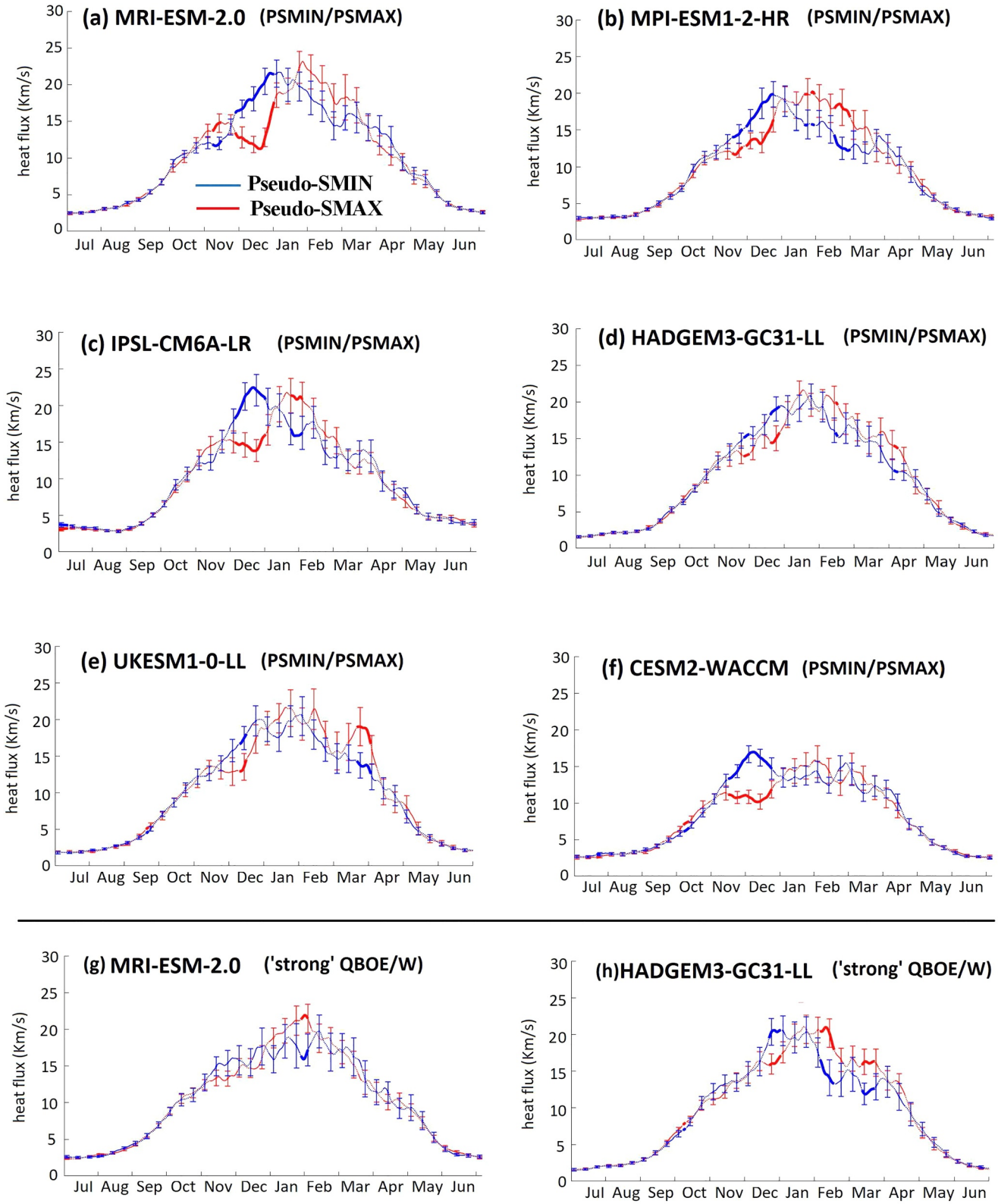

Figure 9. Time series of composited pseudo-SMIN/SMAX (Dec) (a–f) and 'strong' QBOE/W (g–h) (blue/red curves) $[v^*T^*]$ 100-hPa values, averaged over 45°N–75°N and smoothed using a 15-day running mean filter. Models are as indicated, with (a–f) using the 'original' data sets, and (g–h) the 'expanded' data sets, as detailed in Section 2.1. Solid, dotted, and bold curves and error bars are as in Figure 2.

In general terms, however, certain model deficiencies appear to be shared: most model QBOs at 50 hPa (all except WACCM) have westerly biases, with often weak and transient easterlies, leading to few QBOE winters according to the 'strict' criteria. This westerly bias is consistent with findings from previous studies of CMIP6 models (e.g., Richter et al., 2020). All have very weak stratospheric cooling/heating in response to solar forcing, leading to no alterations in the upper stratospheric subtropical jet. All fail to reproduce a full and strong solar/QBO modulation of extratropical wave fluxes, with most (all except MRI and MPI) failing to produce any impact of SMIN/QBOE on early winter wave propagation. Finally, most models, whilst producing some static stability reduction in response to increased wave fluxes in early winter (all except WACCM), tend to produce static stability reductions that are too small and/or short in duration to have any impact upon the MJO. This latter assertion is based on the fact that, in Section 3.6, significant, if brief, MJO amplifications were achieved in the MPI and HADGEM models in response to early SSWs with significant accompanying static stability reductions (Figure 7a–b, e–f). Further, the first two model deficiencies listed above might be responsible for the third one, that is, improvements in the 50-hPa QBO easterly phases and solar-induced stratospheric cooling/heating may lead to better QBO/solar modulation of extratropical wave fluxes. This possibility is supported by the improved HT effect seen in the MRI and HADGEM models when stronger threshold values are imposed upon the QBOE winds (see Figures 9g and 9h and Tables S2–S3 in Supporting Information S1), and the pseudo-solar modulation of extratropical wave activity seen when the models are filtered for early winters with a strong/weak upper stratospheric subtropical westerly jet (see Figures 9a–9f).

Furthermore, with none of the models except WACCM producing strong, significant, and persistent OMI increases in response to equatorial tropopause static stability reductions (see Figures 5b–5f), it is also clear that improvements need to be made to the modeled MJOs, perhaps requiring an improvement to their convective parameterization(s) (e.g., Chen et al., 2021), and/or changes to the absolute static stability values, such that they are closer to observations and more capable of triggering changes in the MJO. This latter statement is supported by analyses of the MRI model 4 $\times$ CO_2 simulations (HTG23), which had significantly lower climatological midwinter static stabilities than the historical simulations analyzed here. Specifically, as shown in Figure 1b, Figures S1b, S2b, S5b, and S10 in Supporting Information S1, the historical MRI simulation produced no discernible MJO modulation by the QBO, solar cyle, or early SSWs, even when the latter were filtered for SSWs which produced significant static stability reductions (see Figure S10 in Supporting Information S1). On the other hand, the MRI 4 $\times$ CO_2 simulation was able to produce a lagged amplification of the MJO following early winter SSWs with large static stability reductions (Figures 7 and 8 of HTG23).

However, it should be emphasized that there are some caveats to these results. First, despite the high inverse correlation between early winter extratropical wave forcing anomalies and DJF mean static stability in the tropical lower stratosphere, there is only a weak correlation in a given QBO phase between the wave forcing anomalies and MJO amplitude (Figure 3a of HTG23). Second, data selection may produce aliasing between signals that leads to uncertainty regarding the direction of causality. For example, in HTG23, the result that early winter SSWs lead to a stronger MJO response than SSWs in late winter was interpreted to be because early winter SSWs occur as tropical lower stratospheric static stability is approaching its midwinter minimum. But it could be argued that early winter SSWs occur preferentially in QBOE because of the HT effect and that the QBO-induced meridional circulation, which is stronger in QBOE, separately produces lower static stability independent of the SSWs. Thus, the larger effects of early SSWs might be because they are more likely to occur during QBOE, which has lower static stability because of the QBO-induced meridional circulation, and not necessarily because the early SSWs occur near (or prior to) the minimum in static stability. More work is therefore needed to verify that the early winter SSW wave forcing events are really producing the lagged increase in MJO amplitude and that this is occurring independently of the effects of the QBO-induced meridional circulation.

Moreover, support for the conclusion that climatological DJF static stability is predictive of the MJO sensitivity to variations in static stability comes from results for only one or two models. The model with the lowest climatological static stability (WACCM) indeed shows a definite relationship between static stability and MJO amplitude (Figure 5g). However, the model with the next lowest static stability (MPI) has only a weak relationship between static stability and the MJO (Figure 5c). Clearly, either a larger sample size of models or more detailed analyses of the selected models is needed to provide a stronger statistical basis for the sensitivity of MJO amplitude to static stability. Perhaps only then would model developers be justified in devoting a large focus on the controlling factors of static stability in the tropical lower stratosphere. Furthermore, the proxy variable defining pseudo-SMIN and pseudo-SMAX in this analysis (i.e., Northern Hemisphere subtropical winds at the

stratopause) could itself be correlated with the QBO. The subtropical winds at 1 hPa are inversely correlated with 10-hPa equatorial winds (see, e.g., Figure 10 of Smith et al., 2023). The latter winds are in turn inversely correlated with equatorial winds near 50 hPa where the QBO is defined. Hence, more easterly winds at the stratopause (labeled SMIN) could potentially be aliased with QBOE conditions on the 11-year timescale (although this would not apply to the 27-day timescale).

Finally, whilst these results lend some support to the proposed mechanism, they do not preclude the possibility that other, additional mechanisms may be involved. In particular, it is very conceivable that cloud-radiative feedback may be necessary to amplify the QBO-induced temperature/static stability anomalies, such that they are capable of strengthening/weakening the MJO to the observed extent (e.g., Son et al., 2017). This would be in agreement with Huang et al. (2023), who found that QBO-induced temperature anomalies—whilst capable of producing a strengthened MJO in a subseasonal-to-seasonal model—were alone not enough to produce the full MJO amplification seen in observations.

Data Availability Statement

The ERA5 1979–2021 data (Hersbach et al., 2020) used for analyses in Section 3 were obtained via ECMWF's online Climate Data Store, and can be accessed freely via https://doi.org/10.24381/cds.bd0915c6 and https://doi.org/10.24381/cds.adbb2d47 (Hersbach et al., 2023a, Hersbach et al., 2023b). The FUB equatorial zonal wind values used for comparison with the ERA5 data were obtained via the Free University of Berlin website, and can be downloaded from https://www.geo.fu-berlin.de/met/ag/strat/produkte/qbo/qbo.dat.

The data from the MRI, MPI, IPSL, HADGEM, UKESM, and WACCM CMIP6 historical model simulations used for analysis in Section 3 were obtained from the Earth System Grid Federation (ESGF) online CMIP6 data repository, and can be accessed under the Creative Commons 4.0 license via https://doi.org/10.22033/ESGF/CMIP6.6842, https://doi.org/10.22033/ESGF/CMIP6.5195, https://doi.org/10.22033/ESGF/CMIP6.10071, https://doi.org/10.22033/ESGF/CMIP6.6594, https://doi.org/10.22033/ESGF/CMIP6.6109, and https://doi.org/10.22033/ESGF/CMIP6.6113 (Boucher et al., 2018; Danabasoglu, 2019; Danabasoglu et al., 2020; Jungclaus et al., 2019; Ridley et al., 2019; Tang et al., 2019; Yukimoto, Kawai, et al., 2019; Yukimoto, Koshiro, et al., 2019).

The OMI values used for the ERA5 data were obtained from the data set published by NOAA, and are available at https://psl.noaa.gov/mjo/mjoindex/omi.1x.txt.

For the models, the OMI values were calculated from daily OLR values using the Python code detailed in Hoffmann et al. (2021), available at https://doi.org/10.5281/zenodo.7261815 (Hoffmann, 2022).

Acknowledgments
Support from the NSF Climate and Large-Scale Dynamics program (2039384) and the NASA Living with a Star program (80NSSC21K1309) is appreciated. Thanks to Thomas Galarneau for his help in retrieving the data from the WACCM model simulations, to Rolando Garcia in providing information about those model simulations, and to Charles Andrew Hoopes and Jacob van der Leeuw for their assistance in OMI calculations for model data. Special thanks to the three reviewers for their critical comments and suggestions, which significantly improved the paper.

References

Ahn, M. S., Kim, D., Kang, D., Lee, J., Sperber, K. R., Gleckler, P. J., et al. (2020). MJO propagation across the Maritime Continent: Are CMIP6 models better than CMIP5 models? *Geophysical Research Letters*, *47*(11), e2020GL087250. https://doi.org/10.1029/2020GL087250

Ambaum, M., & Hoskins, B. (2002). The NAO troposphere-stratosphere connection. *Journal of Climate*, *15*(14), 1969–1978. https://doi.org/10.1175/1520-0442(2002)015<1969:TNTSC>2.0.CO;2

Andrews, M. B., Knight, J. R., Scaife, A., Lu, Y., Wu, T., Gray, L. J., & Schenzinger, V. (2019). Observed and simulated teleconnections between the stratospheric quasi-biennial oscillation and Northern Hemisphere winter atmospheric circulation. *Journal of Geophysical Research: Atmospheres*, *124*(3), 1219–1232. https://doi.org/10.1029/2018JD029368

Anstey, J. A., & Shepherd, T. G. (2014). High-latitude influence of the quasi-biennial oscillation. *Quarterly Journal of the Royal Meteorological Society*, *140*(678), 1–21. https://doi.org/10.1002/qj.2132

Baldwin, M. P., & Dunkerton, T. J. (2001). Stratospheric harbingers of anomalous weather regimes. *Science*, *294*(5542), 581–584. https://doi.org/10.1126/science.1063315

Boucher, O., Denvil, S., Levavasseur, G., Cozic, A., Caubel, A., Foujols, M.-A., et al. (2018). *IPSL IPSL-CM6A-LR model output prepared for CMIP6 CMIP historical*. Earth System Grid Federation. https://doi.org/10.22033/ESGF/CMIP6.5195

Boucher, O., Servonnat, J., Albright, A. L., Aumont, O., Balkanski, Y., Bastrikov, V., et al. (2020). Presentation and evaluation of the IPSL-CM6A-LR climate model. *Journal of Advances in Modeling Earth Systems*, *12*(7), e2019MS002010. https://doi.org/10.1029/2019MS002010

Charlton, A. J., & Polvani, L. M. (2007). A new look at stratospheric sudden warmings. Part I: Climatology and modeling benchmarks. *Journal of Climate*, *20*(3), 449–469. https://doi.org/10.1175/JCLI3996.1

Chen, C. C., Richter, J. H., Liu, C., Moncrieff, M. W., Tang, Q., Lin, W., et al. (2021). Effects of organized convection parameterization on the MJO and precipitation in E3SMv1. Part I: Mesoscale heating. *Journal of Advances in Modeling Earth Systems*, *13*(6), e2020MS002401. https://doi.org/10.1029/2020MS002401

Collimore, C. C., Martin, D. W., Hitchman, M. H., Huesmann, A., & Waliser, D. E. (2003). On the relationship between the QBO and tropical deep convection. *Journal of Climate*, *16*(15), 2552–2568. https://doi.org/10.1175/1520-0442(2003)016<2552:OTRBTQ>2.0.CO;2

Danabasoglu, G. (2019). *NCAR CESM2-WACCM model output prepared for CMIP6 CMIP historical*. Earth System Grid Federation. https://doi.org/10.22033/ESGF/CMIP6.10071

Danabasoglu, G., Lamarque, J. F., Bacmeister, J., Bailey, D. A., DuVivier, A. K., Edwards, J., et al. (2020). The community earth system model version 2 (CESM2). *Journal of Advances in Modeling Earth Systems*, *12*(2), e2019MS001916. https://doi.org/10.1029/2019MS001916

Elsbury, D., Peings, Y., & Magnusdottir, G. (2021). CMIP6 models underestimate the holton-tan effect. *Geophysical Research Letters*, *48*(24), e2021GL094083. https://doi.org/10.1029/2021GL094083

Eyring, V., Bony, S., Meehl, G. A., Senior, C. A., Stevens, B., Stouffer, R. J., & Taylor, K. E. (2016). Overview of the coupled model Intercomparison Project phase 6 (CMIP6) experimental design and organization. *Geoscientific Model Development*, *9*(5), 1937–1958. https://doi.org/10.5194/gmd-9-1937-2016

Garfinkel, C. I., Shaw, T. A., Hartmann, D. L., & Waugh, D. W. (2012). Does the Holton–Tan mechanism explain how the quasi-biennial oscillation modulates the Arctic polar vortex? *Journal of the Atmospheric Sciences*, *69*(5), 1713–1733. https://doi.org/10.1175/JAS-D-11-0209.1

Gettelman, A., Mills, M. J., Kinnison, D. E., Garcia, R. R., Smith, A. K., Marsh, D. R., et al. (2019). The whole atmosphere community climate model version 6 (WACCM6). *Journal of Geophysical Research: Atmospheres*, *124*(23), 12380–12403. https://doi.org/10.1029/2019JD030943

Gray, L. J., Anstey, J. A., Kawatani, Y., Lu, H., Osprey, S., & Schenzinger, V. (2018). Surface impacts of the quasi biennial oscillation. *Atmospheric Chemistry and Physics*, *18*(11), 8227–8247. https://doi.org/10.5194/acp-18-8227-2018

Gray, L. J., Beer, J., Geller, M., Haigh, J. D., Lockwood, M., Matthes, K., et al. (2010). Solar influences on climate. *Reviews of Geophysics*, *48*(4). https://doi.org/10.1029/2009RG000282

Gray, L. J., Crooks, S., Pascoe, C., Sparrow, S., & Palmer, M. (2004). Solar and QBO influences on the timing of stratospheric sudden warmings. *Journal of the Atmospheric Sciences*, *61*(23), 2777–2796. https://doi.org/10.1175/JAS-3297.1

Haigh, J. D., Blackburn, M., & Day, R. (2005). The response of tropospheric circulation to perturbations of lower-stratospheric temperature. *Journal of Climate*, *18*(17), 3672–3685. https://doi.org/10.1175/JCLI3472.1

Hansen, F., Matthes, K., & Gray, L. J. (2013). Sensitivity of stratospheric dynamics and chemistry to QBO nudging width in the chemistry-climate model WACCM. *Journal of Geopjysical Research: Atmosphere*, *118*(18), 10464–10474. https://doi.org/10.1002/jgrd.50812

Haynes, P. H., Marks, C. J., McIntyre, M. E., Shepherd, T. G., & Shine, K. P. (1991). On the "downward control" of extratropical diabatic circulations by eddy-induced mean zonal forces. *Journal of the Atmospheric Sciences*, *48*(4), 651–678. https://doi.org/10.1175/1520-0469(1991)048<0651:OTCOED>2.0.CO;2

Hendon, H. H., & Abhik, S. (2018). Differences in vertical structure of the Madden-Julian Oscillation associated with the quasi-biennial oscillation. *Geophysical Research Letters*, *45*(9), 4419–4428. https://doi.org/10.1029/2018GL077207

Hersbach, H., Bell, B., Berrisford, P., Biavati, G., Horányi, A., Muñoz Sabater, J., et al. (2023a). ERA5 hourly data on pressure levels from 1940 to present. *Copernicus Climate Change Service (C3S) Climate Data Store (CDS)*. [Dataset]. https://doi.org/10.24381/cds.bd0915c6

Hersbach, H., Bell, B., Berrisford, P., Biavati, G., Horányi, A., Muñoz Sabater, J., et al. (2023b). ERA5 hourly data on single levels from 1940 to present. *Copernicus Climate Change Service (C3S) Climate Data Store (CDS)*. [Dataset]. https://doi.org/10.24381/cds.adbb2d47

Hersbach, H., Bell, B., Berrisford, P., Hirahara, S., Horányi, A., Muñoz-Sabater, J., et al. (2020). The ERA5 global reanalysis. *Quarterly Journal of the Royal Meteorological Society*, *146*(730), 1999–2049. https://doi.org/10.1002/qj.3803

Hoffmann, C. G. (2022). Mjoindices October 28, 2022 release (Version 1.4.1) [Software]. *Zenodo*. https://doi.org/10.5281/zenodo.7261815

Hoffmann, C. G., Kiladis, G. N., Gehne, M., & von Savigny, C. (2021). A Python package to calculate the OLR-based Index of the madden-julian-oscillation (OMI) in climate science and weather forecasting. *Journal of Open Research Software*, *9*(1), 9. https://doi.org/10.5334/jors.331

Hoffmann, C. G., & von Savigny, C. (2019). Indications for a potential synchronization between the phase evolution of the Madden–Julian oscillation and the solar 27-day cycle. *Atmospheric Chemistry and Physics*, *19*(7), 4235–4256. https://doi.org/10.5194/acp-19-4235-2019

Holton, J. R., & Tan, H. C. (1980). The influence of the equatorial quasi-biennial oscillation on the global circulation at 50 mb. *Journal of the Atmospheric Sciences*, *37*(10), 2200–2208. https://doi.org/10.1175/1520-0469(1980)037<2200:TIOTEQ>2.0.CO;2

Hood, L. L. (2017). QBO/solar modulation of the boreal winter madden-julian oscillation: A prediction for the coming solar minimum. *Geophysical Research Letters*, *44*(8), 3849–3857. https://doi.org/10.1002/2017GL072832

Hood, L. L. (2018). Short-term solar modulation of the Madden–Julian climate oscillation. *Journal of the Atmospheric Sciences*, *75*(3), 857–873. https://doi.org/10.1175/JAS-D-17-0265.1

Hood, L. L., & Hoopes, C. A. (2023). Arctic sea ice loss, long-term trends in extratropical wave forcing, and the observed strengthening of the QBO-MJO connection. *Journal of Geophysical Research*, *128*(24). https://doi.org/10.1029/2023JD039501

Hood, L. L., Misios, S., Mitchell, D. M., Rozanov, E., Gray, L. J., Tourpali, K., et al. (2015). Solar signals in CMIP-5 simulations: The ozone response. *Quarterly Journal of the Royal Meteorological Society*, *141*(692), 2670–2689. https://doi.org/10.1002/qj.2553

Hood, L. L., Trencham, N. E., & Galarneau Jr, T. J. (2023). QBO/Solar influences on the tropical madden-julian oscillation: A mechanism based on extratropical wave forcing in late fall and early winter. *Journal of Geophysical Research: Atmospheres*, *128*(6), e2022JD037824. https://doi.org/10.1029/2022JD037824

Hoopes, C. A., Hood, L. L., & Galarneau, T. J., Jr. (2024). Lagged response of MJO convection and precipitation to solar ultraviolet variations on intraseasonal time scales. *Geophysical Research Letters*, *51*(11), e2023GL107701. https://doi.org/10.1029/2023GL107701

Houghton, J. T. (1977). *The physics of atmospheres* (p. 203). Cambridge University Press.

Huang, K., Richter, J. H., & Pegion, K. V. (2023). Captured QBO-MJO connection in a subseasonal prediction system. *Geophysical Research Letters*, *50*(8), e2022GL102648. https://doi.org/10.1029/2022GL102648

Jungclaus, J., Bittner, M., Wieners, K.-H., Wachsmann, F., Schupfner, M., Legutke, S., et al. (2019). *MPI-M MPI-ESM1.2-HR model output prepared for CMIP6 CMIP historical*. Earth System Grid Federation. https://doi.org/10.22033/ESGF/CMIP6.6594

Kiladis, G. N., Dias, J., Straub, K. H., Wheeler, M. C., Tulich, S. N., Kikuchi, K., et al. (2014). A comparison of OLR and circulation-based indices for tracking the MJO. *Monthly Weather Review*, *142*(5), 1697–1715. https://doi.org/10.1175/MWR-D-13-00301.1

Kim, H., Caron, J. M., Richter, J. H., & Simpson, I. R. (2020). The lack of QBO-MJO connection in CMIP6 models. *Geophysical Research Letters*, *47*(11), e2020GL087295. https://doi.org/10.1029/2020GL087295

Kodera, K., & Kuroda, Y. (2002). Dynamical response to the solar cycle. *Journal of Geophysical Research*, *107*(D24). ACL-5. https://doi.org/10.1029/2002JD002224

Kodera, K., Nasuno, T., Son, S.-W., Eguchi, N., & Harada, Y. (2023). Influence of the stratospheric QBO on seasonal migration of the convective center across the Maritime Continent. *Journal of the Meteorological Society of Japan*, *101*(6), 445–459. https://doi.org/10.2151/jmsj.2023-026

LaMorte, W. H. (2021). *Confidence intervals for sample size less than 30, PH717 Module 6 – random error, probability, estimation, and confidence intervals*. Boston University School of Public Health. Retrieved from https://sphweb.bumc.bu.edu/otlt/MPH-Modules/PH717-QuantCore/PH717-Module6-RandomError/PH717-Module6-RandomError11.html

Lim, Y., & Son, S.-W. (2022). QBO wind influence on MJO-induced temperature anomalies in the upper troposphere and lower stratosphere in an idealized model. *Journal of the Atmospheric Sciences*, *79*(9), 2219–2228. https://doi.org/10.1175/JAS-D-21-0296.1

Lu, H., Hitchman, M. H., Gray, L. J., Anstey, J. A., & Osprey, S. M. (2020). On the role of Rossby wave breaking in the quasi-biennial modulation of the stratospheric polar vortex during boreal winter. *Quarterly Journal of the Royal Meteorological Society*, *146*(729), 1939–1959. https://doi.org/10.1002/qj.3775

Martin, Z., Orbe, C., Wang, S., & Sobel, A. (2021). The MJO–QBO relationship in a GCM with stratospheric nudging. *Journal of Climate*, *34*(11), 4603–4624. https://doi.org/10.1175/JCLI-D-20-0636.1

Martin, Z., Son, S.-W., Butler, A., Hendon, H., Kim, H., Sobel, A., et al. (2021). The influence of the quasi-biennial oscillation on the Madden-Julian oscillation. *Nature Reviews Earth and Environment*, *2*(7), 477–489. https://doi.org/10.1038/s43017-021-00173-9

Martin, Z., Wang, S., Nie, J., & Sobel, A. (2019). The impact of the QBO on MJO convection in cloud-resolving simulations. *Journal of the Atmospheric Sciences*, *76*(3), 669–688. https://doi.org/10.1175/JAS-D-18-0179.1

Martin, Z. K., Simpson, I. R., Lin, P., Orbe, C., Tang, Q., Caron, J. M., et al. (2023). The lack of a QBO-MJO connection in climate models with a nudged stratosphere. *Journal of Geophysical Research: Atmospheres*, *128*(17), e2023JD038722. https://doi.org/10.1029/2023JD038722

Mitchell, D. M., Misios, S., Gray, L. J., Tourpali, K., Matthes, K., Hood, L., et al. (2015). Solar signals in CMIP-5 simulations: The stratospheric pathway. *Quarterly Journal of the Royal Meteorological Society*, *141*(691), 2390–2403. https://doi.org/10.1002/qj.2530

Müller, W. A., Jungclaus, J. H., Mauritsen, T., Baehr, J., Bittner, M., Budich, R., et al. (2018). A higher-resolution version of the max planck institute earth system model (MPI-ESM1.2-HR). *Journal of Advances in Modeling Earth Systems*, *10*(7), 1383–1413. https://doi.org/10.1029/2017MS001217

Newman, P. A., Nash, E. R., & Rosenfield, J. E. (2001). What controls the temperature of the Arctic stratosphere in the spring? *Journal of Geophysical Research*, *106*(D17), 19999–20010. https://doi.org/10.1029/2000JD000061

Nishimoto, E., & Yoden, S. (2017). Influence of the stratospheric quasi-biennial oscillation on the Madden–Julian oscillation during austral summer. *Journal of the Atmospheric Sciences*, *74*(4), 1105–1125. https://doi.org/10.1175/JAS-D-16-0205.1

Peixoto, J. P., & Oort, A. H. (1992). *Physics of climate* (1st ed.). American Institute of Physics.

Polvani, L. M., & Waugh, D. W. (2004). Upward wave activity flux as a precursor to extreme stratospheric events and subsequent anomalous surface weather regimes. *Journal of Climate*, *17*(18), 3548–3554. https://doi.org/10.1175/1520-0442(2004)017<3548:UWAFAA>2.0.CO;2

Rao, J., Garfinkel, C. I., & White, I. P. (2020). Impact of the quasi-biennial oscillation on the northern winter stratospheric polar vortex in CMIP5/6 models. *Journal of Climate*, *33*(11), 4787–4813. https://doi.org/10.1175/JCLI-D-19-0663.1

Richter, J. H., Anstey, J. A., Butchart, N., Kawatani, Y., Meehl, G. A., Osprey, S., & Simpson, I. R. (2020). Progress in simulating the quasi-biennial oscillation in CMIP models. *Journal of Geophysical Research: Atmospheres*, *125*(8), e2019JD032362. https://doi.org/10.1029/2019JD032362

Ridley, J., Menary, M., Kuhlbrodt, T., Andrews, M., & Andrews, T. (2019). *MOHC HadGEM3-GC31-LL model output prepared for CMIP6 CMIP historical*. Earth System Grid Federation. https://doi.org/10.22033/ESGF/CMIP6.6109

Sakaeda, N., Dias, J., & Kiladis, G. N. (2020). The unique characteristics and potential mechanisms of the MJO-QBO relationship. *Journal of Geophysical Research: Atmospheres*, *125*(17), e2020JD033196. https://doi.org/10.1029/2020JD033196

Sellar, A. A., Jones, C. G., Mulcahy, J. P., Tang, Y., Yool, A., Wiltshire, A., et al. (2019). UKESM1: Description and evaluation of the UK earth system model. *Journal of Advances in Modeling Earth Systems*, *11*(12), 4513–4558. https://doi.org/10.1029/2019MS001739

Simpson, I. R., Blackburn, M., & Haigh, J. D. (2009). The role of eddies in driving the tropospheric response to stratospheric heating perturbations. *Journal of the Atmospheric Sciences*, *66*(5), 1347–1365. https://doi.org/10.1175/2008JAS2758.1

Smith, A. K., Gray, L. J., & Garcia, R. R. (2023). Evidence for the influence of the quasi-biennial oscillation on the semiannual oscillation in the tropical middle atmosphere. *Journal of the Atmospheric Sciences*, *80*(7), 1755–1769. https://doi.org/10.1175/JAS-D-22-0255.1

Son, S. W. (2023). QBO-MJO connection: Two possible mechanisms. In *Paper presented at QBO workshop*. Oxford University. 27-31 March, 2023.

Son, S.-W., Lim, Y., Yoo, C., Hendon, H. H., & Kim, J. (2017). Stratospheric control of madden–julian oscillation. *Journal of Climate*, *30*(6), 1909–1922. https://doi.org/10.1175/JCLI-D-16-0620.1

Tang, Y., Rumbold, S., Ellis, R., Kelley, D., Mulcahy, J., Sellar, A., et al. (2019). *MOHC UKESM1.0-LL model output prepared for CMIP6 CMIP historical*. Earth System Grid Federation. https://doi.org/10.22033/ESGF/CMIP6.6113

White, I. P., Lu, H., Mitchell, N. J., & Phillips, T. (2015). Dynamical response to the QBO in the northern winter stratosphere: Signatures in wave forcing and eddy fluxes of potential vorticity. *Journal of the Atmospheric Sciences*, *72*(12), 4487–4507. https://doi.org/10.1175/JAS-D-14-0358.1

Williams, K. D., Copsey, D., Blockley, E. W., Bodas-Salcedo, A., Calvert, D., Comer, R., et al. (2017). The Met Office global coupled model 3.0 and 3.1 (GC3. 0 and GC3. 1) configurations. *Journal of Advances in Modeling Earth Systems*, *10*(2), 357–380. https://doi.org/10.1002/2017MS001115

Yoo, C., & Son, S. W. (2016). Modulation of the boreal wintertime Madden-Julian oscillation by the stratospheric quasi-biennial oscillation. *Geophysical Research Letters*, *43*(3), 1392–1398. https://doi.org/10.1002/2016GL067762

Yukimoto, S., Kawai, H., Koshiro, T., Oshima, N., Yoshida, K., Urakawa, S., et al. (2019). The meteorological Research institute earth system model version 2.0, MRI-ESM2. 0: Description and basic evaluation of the physical component. *Journal of the Meteorological Society of Japan*, *97*(5), 931–965. https://doi.org/10.2151/jmsj.2019-051

Yukimoto, S., Koshiro, T., Kawai, H., Oshima, N., Yoshida, K., Urakawa, S., et al. (2019). MRI MRI-ESM2.0 model output prepared for CMIP6 CMIP historical. *Earth System Grid Federation*. https://doi.org/10.22033/ESGF/CMIP6.6842

Zhang, C. (2005). Madden-julian oscillation. *Reviews of Geophysics*, *43*(2). https://doi.org/10.1029/2004RG000158

Zhang, C. (2013). Madden–Julian oscillation: Bridging weather and climate. *Bulletin of the American Meteorological Society*, *94*(12), 1849–1870. https://doi.org/10.1175/BAMS-D-12-00026.1